ADVANCED MATERIALS INTERFACES
www.advmatinterfaces.de

Perovskite/Silicon Tandem Solar Cells: Marriage of Convenience or True Love Story? – An Overview

Jérémie Werner, Bjoern Niesen, and Christophe Ballif*

Perovskite/silicon tandem solar cells have reached efficiencies above 25% in just about three years of development, mostly driven by the rapid progress made in the perovskite solar cell research field. This review aims to give an overview of the achievements made in this timeframe toward the goal of developing high-efficiency perovskite/silicon tandem cells with sufficiently large area and long lifetime to be commercially interesting. The developments that led to the recent progress in tandem cell efficiency, as well as the factors currently still limiting their performance, including parasitic absorption, reflection losses, and the nonideal perovskite absorber layer bandgap, are discussed. Based on this discussion, guidelines for future developments are given. In addition, crucial aspects to enable the commercialization of perovskite/silicon tandem solar cells are reviewed, such as device stability and upscaling. Finally, economic considerations show how the number of steps and/or the costs associated to these steps for realizing the perovskite cell must be kept to a minimum to keep up with progress in the field of silicon photovoltaics.

1. Introduction

Harvesting the power of the sun is certainly one of the most promising approaches to supply the world with sustainable, clean, and low-cost energy. In recent years, the cost of photovoltaic (PV) systems has decreased drastically while installations have soared, making PV economically competitive with conventional energy resources, e.g., coal, in many areas. As prices are falling, wholesale and retail grid parity should be reached in most countries within a few years.[1]

For a PV system, the levelized cost of electricity (LCOE) is dominated by the balance-of-system costs (BOS), including inverter, construction, connection, and mounting structure, with a share of typically above 50% of the total costs. Therefore, a straightforward approach to reduce the LCOE is to raise the cell efficiency, which directly lowers the area-related BOS costs (except for the inverter, all other BOS costs are area-related), if implemented without significant additional processing costs.[2]

Crystalline silicon-based technologies are currently dominating the PV market, thanks to their low fabrication costs and high reliability of their material and fabrication processes.[3] Typical module efficiencies are about 17–18%, with a record commercial product efficiency of 22.2%.[4,5] Research cell record efficiencies are approaching 27%, with the latest certified record of Kaneka at 26.6%.[6,7] Therefore, only marginal improvements in performance are still possible, considering the 29.4% theoretical limit for crystalline silicon solar cells.[8] This limit is defined by considering Auger recombination and intrinsic losses such as, among others, the transparency of the absorber layer for sub-bandgap photons and thermalization losses for high-energy photons.[9] As illustrated in **Figure 1**a, the most effective solution to reduce these intrinsic losses is to combine several absorber materials with different bandgaps in a multijunction solar cell. The use of a high bandgap material will allow for a reduction in thermalization losses and collection of remaining nonabsorbed light in a lower bandgap cell will reduce the sub-bandgap losses. The most simple multijunction configuration is the so-called tandem solar cell combining two subcells.

For such tandem cells, crystalline silicon solar cells are nearly ideal in the role of the low bandgap bottom cell due to their suitable bandgap of 1.1 eV, high open-circuit voltage (V_{OC}) of up to 750 mV,[10] cost-competitive manufacturing based on their market dominance, and high efficiency.[7] Finding its ideal wide-bandgap partner is considerably more difficult. III–V solar cells have been proposed for their high efficiency and tunable bandgap, and mechanically stacked four-terminal tandem cells with >32% efficiency were recently demonstrated.[11] However, the high manufacturing costs of III–V solar cells hinder their large-scale deployment for terrestrial applications. A possible answer to this quest for high efficiency and low cost came with the emergence of perovskite solar cells.[12,13]

Organic–inorganic lead halide perovskite solar cells present several advantages that make them highly interesting for their use as a top cell in silicon-based tandem solar cells. The performance of perovskite cells has been rapidly raised to 22.1%,[14] with an increasing number of research groups showing >20% efficient cells.[15–19] Their exceptional optoelectronic properties are also well suited for tandem applications, including a high

J. Werner, Dr. B. Niesen, Prof. C. Ballif
Photovoltaics and Thin-Film Electronics Laboratory
Institute of Microengineering (IMT)
Ecole Polytechnique Fédérale de Lausanne (EPFL)
Rue de la Maladiére 71b, 2002 Neuchâtel, Switzerland
E-mail: jeremie.werner@epfl.ch
Dr. B. Niesen, Prof. C. Ballif
CSEM PV-Center
Centre Suisse d'Electronique et de Microtechnique (CSEM)
Jaquet-Droz 1, CH-2002 Neuchâtel, Switzerland

DOI: 10.1002/admi.201700731

absorption coefficient, low sub-bandgap absorption, and a steep absorption edge.[20] Moreover, perovskite solar cells offer bandgap tunability throughout a wide spectral range,[21] high V_{OC} with low potential loss,[22] high defect tolerance, long charge carrier diffusion lengths,[23] and photon recycling.[24] Importantly, perovskite solar cells combine high efficiencies and excellent optoelectronic properties with the potential for low-cost processing and abundant availability of the constituent elements.[25,26] Reported fabrication protocols for perovskite solar cells include a variety of deposition techniques based on solution processes, such as spin coating[17] or slot-die coating,[27] as well as vacuum-based methods, such as thermal evaporation[28] or chemical vapor deposition.[29]

In this review article, we aim to give an overview specifically focused on the development of perovskite/silicon tandem solar cells over the last three years, as compared to other more general reviews published recently.[30,31] We first present the various device architectures that are under research and compare their advantages and disadvantages. Three years of development may not seem long in research. However, this field has already seen tremendous progress (see Figure 1b), which is summarized in Section 3, highlighting the most important steps toward the latest efficiency records. Fortunately, for the scientific community, not everything is done yet: many challenges remain to be solved to further enhance performance toward the theoretical limits (Section 4) and to make this technology ready for commercialization (Section 5).

2. Tandem Architectures

A tandem solar cell can be made in several configurations, each of them having specific advantages and disadvantages, which will hereafter shortly be introduced and compared.

The most simple tandem device architecture from a process development point of view is the mechanically stacked four-terminal tandem (**Figure 2**a). The two subcells are fabricated independently, stacked on top of each other and contacted individually. This has the obvious advantage of process

Jérémie Werner received a M.Sc. degree in Materials Science and Engineering from the Ecole Polytechnique Fédérale de Lausanne, Lausanne, Switzerland, in 2014. He joined the Photovoltaics and Thin-Film Electronics Laboratory, Neuchâtel, Switzerland in July 2014, and has been working toward the Ph.D. degree. His research focuses on the development of high-efficiency perovskite/silicon tandem solar cells.

Bjoern Niesen earned his M.Sc. degree in Nanosciences in 2008 from the University of Basel, Switzerland. In 2012, he received his Ph.D. degree from the Katholieke Universiteit Leuven in Belgium, while he was at the Interuniversity Microelectronics Center (IMEC), working on plasmonics for organic solar cells. Since 2012, he has been at the Photovoltaics and Thin-Film Electronics Laboratory at the École Polytechnique Fédérale de Lausanne (EPFL) in Neuchâtel, Switzerland, where he initially worked on thin-film silicon multijunction solar cells and currently leads the development of perovskite solar cells for high-efficiency tandem cells. Since 2015, he has also been affiliated with the Centre Suisse d'Electronique et de Microtechnique (CSEM) PV-Center in Neuchâtel, Switzerland.

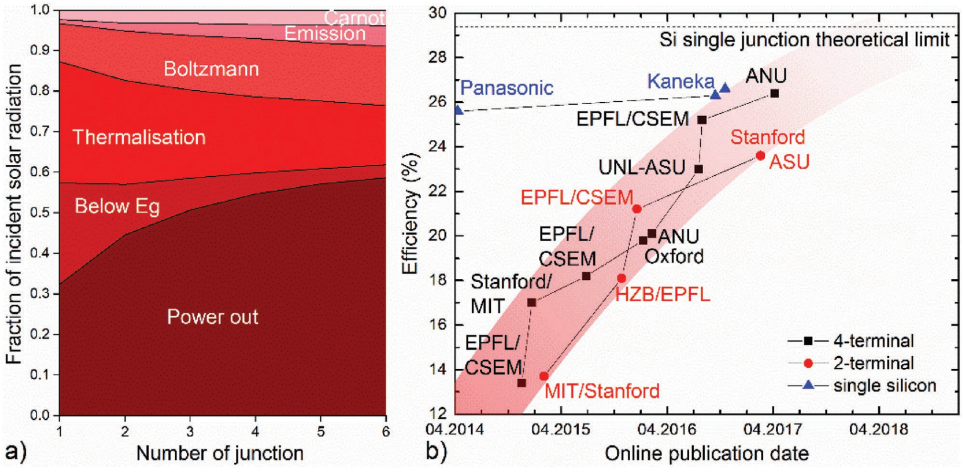

Figure 1. a) Evolution of the fundamental losses in a solar cell when increasing the number of junctions. Adapted with permission.[9] b) Monolithic two-terminal and mechanically stacked four-terminal perovskite/silicon tandem efficiency record evolution, according to the online publication date.

simplicity, allowing for the use of the optimal fabrication conditions specific to each subcell, e.g., concerning cell polarity, substrate roughness, process temperature, and solvents. This configuration requires four electrodes, with at least three of them showing high transparency in a wide spectral range for the front window electrode and at least in the infrared spectral region for the other two. Minimizing parasitic absorption and manufacturing costs for these electrodes is therefore crucial for the viability of this tandem configuration. During operation, the two subcells can be independently kept at their maximum power points, with separate tracking systems. This in particular reduces the constraints on the choice of the top cell bandgap and makes the system less sensitive to spectral variations. As a result, four-terminal tandem cells can reach high efficiencies with a broad range of top cell bandgaps ranging from 1.6 to 2 eV, with an optimum at 1.81 eV when using a crystalline silicon bottom cell.[32] However, using four terminals implies also doubling all the power electronics, e.g., inverters, which comes at a cost. As a possible solution to this problem, mechanically stacked voltage-matched tandem modules have been proposed, using only two terminals and arranging the cells in submodules connected in parallel.[33,34] As the open-circuit voltage varies logarithmically with light intensity, a voltage-matched connection can be more resilient toward spectral variations compared to a current-matched connection.

Other four-terminal tandem concepts were demonstrated, such as spectral splitting systems[35–37] or reflective tandems.[38,39] A four-terminal spectral splitting tandem device consists of a dichroic mirror, which splits the light toward the high and low bandgap cells, as illustrated in Figure 2c. This has the advantage that standard cells can be used without any specific adaptation, particularly without the need for additional transparent electrodes. However, the optical components are usually expensive, limiting the economic viability of this tandem architecture for nonconcentrated photovoltaic systems. Reflective tandems could be an interesting alternative. The PVMirror concept, introduced recently,[39] consists of placing the cheapest subcell in a curved arrangement and use either a short-pass or a long-pass dichroic mirror to reflect and concentrate, respectively, the long or short wavelengths of light onto the more expensive subcell. The concept therefore offers high flexibility in terms of manufacturing and system integration, as it can be combined with other solar energy harvesting technologies, e.g., solar thermal collectors. However, such approaches, which require solar tracking, will be poor at collecting the diffuse light present in the solar spectrum, and their performance might strongly be impacted by module soiling.

Due to the limitations and the rather complex system integration for spectral splitting and reflective tandem cells, we will set the focus of this review on two-terminal and four-terminal planar modules.

Figure 2b presents a monolithically integrated two-terminal perovskite/silicon tandem solar cell. This architecture consists of a perovskite top cell, which is deposited onto the silicon

Christophe Ballif received the Graduate's degree in physics and Ph.D. degree from the Ecole Polytechnique Fédérale de Lausanne (EPFL), Lausanne, Switzerland, in 1994 and 1998, respectively, focusing on novel photovoltaic materials. He was a Postdoctoral Researcher with the National Renewable Energy Laboratory, Golden, CO, USA. He was then with the Fraunhofer Institute for Solar Energy Systems, Freiburg, Germany, where he was involved in crystalline silicon photovoltaics (monocrystalline and multicrystalline) until 2003. He then joined the Swiss Federal Laboratories for Materials Science and Technology, Dübendorf, Switzerland, before becoming a Full Professor and Chair with the Institute of Microengineering, University of Neuchâtel, Neuchâtel, Switzerland, in 2004. In 2009, the Institute was transferred to EPFL. He is the Director of the Photovoltaics and Thin-Film Electronics Laboratory within the Institute, as well as of the CSEM PV-Center. His research interests include thin-film solar cells, high-efficiency crystalline cells, module technology, building integrated photovoltaic, and system aspects contributing to technology transfer and industrialization of novel devices.

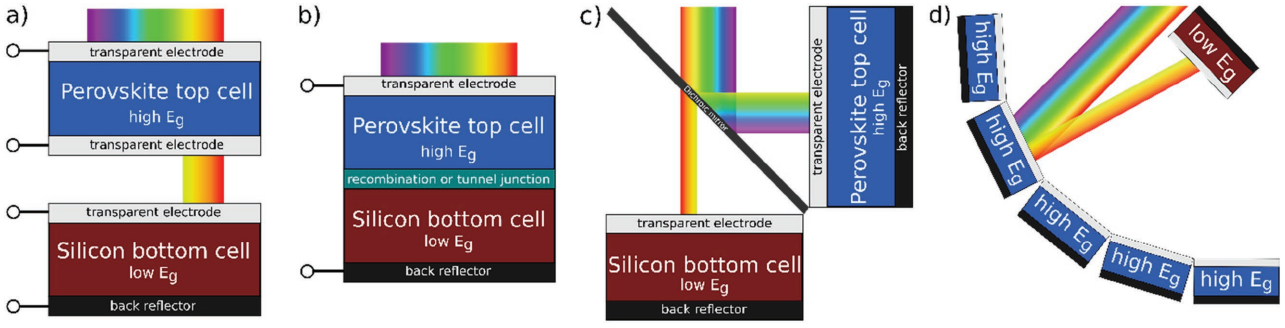

Figure 2. Schematics of several perovskite/silicon tandem architectures: a) four-terminal mechanically stacked; b) two-terminal monolithically integrated; c) four-terminal optical spectral splitting; d) four-terminal reflective tandem. For all these configurations, the perovskite top cell has a higher bandgap (E_g) than the crystalline silicon bottom cell with $E_g = 1.1$ eV.

bottom cell. The two subcells are then electrically connected in series, through a recombination layer or tunnel junction. Compared to the four-terminal mechanically stacked tandem, this architecture therefore requires only one transparent electrode, lowering the manufacturing costs due to reduced material usage and fewer deposition steps. The reduced number of electrodes also leads to less parasitic absorption in the nonactive layers, which is why two-terminal tandems have a high practical efficiency potential. Following Kirchhoff's law, a monolithic tandem will have a voltage equal to the sum of the ones of the two subcells, which is beneficial as high voltages result in reduced resistive losses in PV systems. However, two-terminal tandem cells also have some constraints: The two subcells must be designed to generate similar photocurrent under operation, as the tandem current will be limited by the subcell with the lower current. This current matching requirement limits the ideal top cell bandgap to a narrow range of 1.7–1.8 eV (**Figure 3**) and makes the system also more sensitive to spectral variations, requiring for optimal operation a specific design for a specific geographic location. Finally, as the top cell layers are deposited onto the bottom cell, the top cell processing has to be performed such that the bottom cell performance is not affected. In addition, the bottom cell has to act as a suitable substrate, which is especially challenging for cells with textured surfaces, as it is typically the case for crystalline silicon cells.

Using detailed-balance calculations, including Auger recombination limiting the silicon single junction cells to 29.4%,[8] the theoretically achievable efficiency for perovskite/silicon tandem cells in the two-terminal and four-terminal configurations can be calculated.[41–43] An efficiency limit of about 43% was found for both configurations, with steeply falling values for nonideal top cell bandgaps in case of the two-terminal tandem due to the current matching restriction (Figure 3). The optimal top cell bandgap is considerably broader for the four-terminal configuration as the subcell currents do not have to be matched.

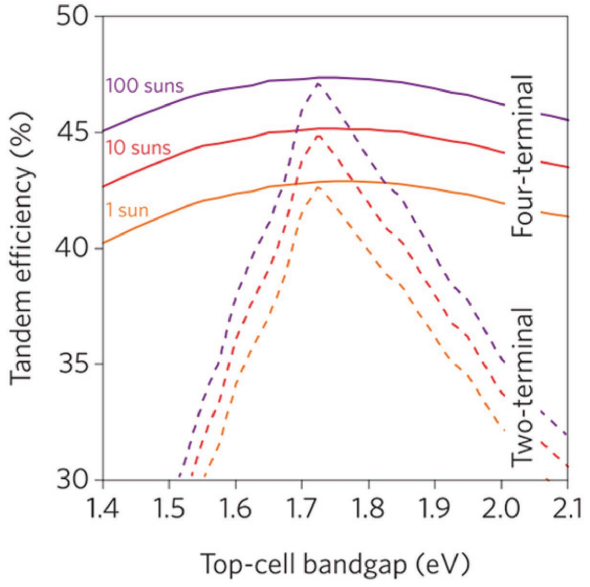

Figure 3. Efficiency limit of two-terminal and four-terminal tandem cells in function of the top-cell bandgap and the illumination intensity. Reproduced with permission.[40] Copyright 2016, Nature Publishing Group.

Perovskite solar cells are suitable partners not only for crystalline silicon but also for emerging thin film technologies, such as chalcogenides,[44–48] kesterites,[49,50] or polymer solar cells.[51] Clear efficiency gains have already been demonstrated, compared to the individual subcell performances, with a record four-terminal tandem efficiency of 22.1% with a CIGS bottom cell.[47] All-perovskite tandems were also already demonstrated. With the recent development of low-bandgap perovskite materials, their performance was rapidly raised to close to 20%.[28,52–57]

On the other hand, silicon solar cells can also be combined with other top cell technologies, such as III–V cells.[11,58] This type of cells has been successfully applied in satellites and terrestrial concentration systems, and allows for high efficiencies with material compositions having ideal top cell bandgaps of 1.7–1.8 eV.[11,58] However, the bottleneck for III–V/silicon tandem cells is the production costs of the top cell: For one-sun terrestrial applications, these tandem cells become economically viable only if the GaAs or InGaP cells can be manufactured at a similar price as the silicon cell,[59] a cost target which has so far not been reached. Nevertheless, III–V/silicon tandems might find use in applications where space constraints (e.g., small roofs) and/or weight saving and power density are more important than achieving the lowest cost.

3. A Bit of History

Even though perovskites have already been studied in the 1990s for light emitting diodes (LEDs) in particular by Mitzi et al.,[60] the first publication showing a solar cell with a perovskite absorber material was published only in 2009 by Miyasaka and co-workers.[61] The efficiency was only 3.8% with a device life time in the range of minutes due to the use of a liquid electrolyte. However, this launched an incredible competition in the photovoltaics research community, leading to a 22.1% certified efficiency in 2016. A dedicated review was recently published elsewhere, providing more in-depth historical details on the birth of the perovskite solar cell.[12]

Perovskite materials quickly triggered interest for multijunction solar cells. Already in his original paper,[61] Miyasaka and co-workers demonstrated high bandgap materials showing high photovoltage and bandgap tunability in the range 1.5-2.1 eV. Later, the possibility to make planar thin film solid-state devices[62] and to use vacuum-based techniques[63] confirmed the potential of this technology to partner with silicon for low-cost tandem cells.[64]

In 2014, De Wolf et al. used photothermal deflection and photocurrent spectroscopy techniques to measure the absorption spectrum of $CH_3NH_3PbI_3$ (MALI), the most widespread perovskite composition.[20] Remarkably, this study showed that this composition has a very large absorption coefficient, with sharp absorption edge and low sub-bandgap absorption, typical of direct semiconductors, such as III–V materials. These optoelectronic properties are essential for a top cell in a tandem solar cell, as they allow for the use of relatively thin absorber layers and lead to minimal parasitic absorption in the sub-bandgap spectral region where light has to be transmitted to the bottom cell.

At the same time, several publications presented simulations based on optical modeling,[41,42,65–67] establishing the requirements and challenges to reach efficiencies beyond 30%. Light management and parasitic absorption were already early identified as major challenges, which will be discussed in more detail in the next section.

The development of any flat plate tandem solar cell in the four-terminal or two-terminal configuration involves replacing the opaque metal rear contact used in single-junction perovskite solar cells with a transparent electrode. The first reports of semitransparent perovskite solar cells and mechanically stacked tandem cells were published at the end of 2014 by Löper et al.[68] and by Bailie et al.,[69] showing 13.4% and 17% four-terminal tandem efficiencies, respectively. Löper and co-workers used a sputtered indium tin oxide (ITO) transparent electrode, which had however suboptimal electronic properties, as the high-temperature treatment normally necessary to reach a low sheet-resistance would have severely damaged the perovskite cell. The same group showed later that using an amorphous transparent conducting oxide (TCO), in this case indium zinc oxide (IZO), instead of ITO can solve this issue as it can be used as-deposited and still has a high carrier mobility and low sheet resistance.[70] Bailie et al. used a silver nanowire mesh, which was first formed by spray coating on a polymer foil and then mechanically transferred onto the perovskite cell layer stack. They could show high transparency and low sheet resistance, but the reproducibility due to the mechanical transfer was still challenging.[69]

Soon after that, this same group collaborated with Buonassisi and co-workers at the Massachusetts Institute of Technology (MIT) to fabricate the first perovskite/silicon monolithic tandem using the same silver nanowire electrode.[71] Using a mesoscopic perovskite top cell and a diffused junction silicon bottom cell with a silicon tunnel junction, they showed a 13.7% efficient monolithic tandem with a still modest V_{OC} of 1.58 V (**Figure 4**a,b). Parasitic absorption in the charge transport layers was drastically limiting the performance of this monolithic tandem device.

These first publications launched an efficiency race, as illustrated in Figure 1b and summarized in **Table 1**, showing the main perovskite/silicon tandem experimental results published in the years 2014–2017.

At the end of 2015, Albrecht et al. first used a silicon heterojunction solar cell as the bottom cell for a monolithic tandem, reaching an efficiency of 18.1%,[80] exploiting their high near-infrared spectral response and high voltage. It was also the first demonstration of a low-temperature planar perovskite solar cell using an atomic layer deposition (ALD)-grown SnO_2 layer as the electron transport layer. The monolithic tandem efficiency record was improved two months later by Werner et al. with a PC fullerene-based planar perovskite top cell and an IZO intermediate recombination layer, reaching a 21.2% steady-state efficiency.[81] This cell was limited by the bottom cell current, due to the use of a double-side polished silicon wafer. In August 2016, the bottom cell current was improved with the introduction of rear-side textured silicon wafers, and an efficiency of

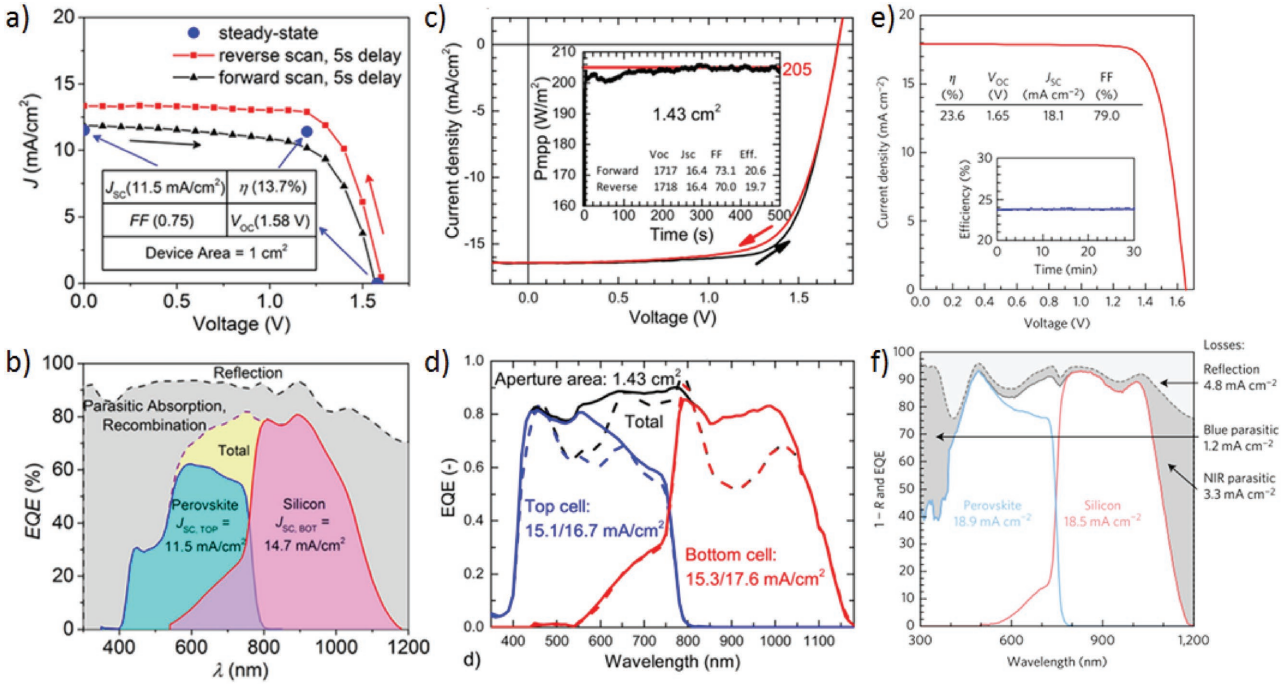

Figure 4. Evolution of perovskite/silicon monolithic tandem solar cells with >1 cm² aperture area: a) *JV* measurements of a two-terminal tandem with a mesoscopic perovskite top cell and b) the corresponding EQE curves. Reproduced with permission.[71] Copyright 2015, AIP Publishing LLC. c) *JV* measurements of a two-terminal tandem with a low-temperature planar perovskite top cell and a rear-side textured silicon heterojunction bottom cell; d) the corresponding EQE curves, of the tandem cell measured either with (solid curves) or without (dashed curves) an antireflective foil. Reproduced with permission.[72] Copyright 2016, American Chemical Society. e,f) *JV* and EQE measurements of the monolithic tandem cell with the current record efficiency of 23.6%. Reproduced with permission.[73] Copyright 2017, Nature Publishing Group.

Table 1. Evolution of four-terminal and two-terminal perovskite/silicon tandem efficiency. *designates steady state efficiencies. SHJ: silicon heterojunction solar cell; PERL: passivated emitter with rear locally diffused solar cell; IBC: interdigitated back contact solar cell; nc-Si: nanocrystalline silicon; IMEC: Interuniversity Microelectronics Center; HZB: Helmholtz-Zentrum Berlin; UNL: University of Nebraska–Lincoln; ASU: Arizona state university; PCE: power conversion efficiency; ZTO: zinc tin oxide.

Mechanically stacked four-terminal						
Perovskite	E_g [eV]	Silicon	Area (top; bottom) [cm^2]	PCE (top + bottom = total) [%]	Institute	Year/reference
$MAPbI_3$	1.55	SHJ	0.25; 4	6.2 + 7.2 = 13.4	EPFL/CSEM	2014/[68]
$MAPbI_3$	1.55	Multi-Si	0.39; 0.39	12.7 + 4.3 = 17.0	Stanford/MIT/EPFL	2014/[69]
$MAPbI_3$	1.55	SHJ	0.25; 4	10.4 + 7.8 = 18.2	EPFL/CSEM	2015/[70]
$FACsPbI_{3-x}Br_x$	1.74	SHJ	0.09; na	12.5 + 7.3 = 19.8*	Oxford/HZB	2016/[74]
$MAPbI_3$	1.55	PERL	0.25; 4	12.2 + 7.9 = 20.1*	ANU	2016/[75]
$MAPbI_3$	1.55	SHJ	0.075; 4	16.5 + 6.5 = 23.0	UNL/ASU	2016/[76]
$MAPbI_3$	1.55	SHJ	0.25; 4	16.4 + 8.8 = 25.2*	EPFL/CSEM	2016/[72]
$MAPbI_3$	1.55	SHJ	1; 4	14.5 + 8.5 = 23.0*	EPFL/CSEM	2016/[72]
$CsMAFAPbI_{3-x}Br_x$	1.63	IBC–SHJ	0.36; 4	16.6 + 7.9 = 24.5*	ANU	2016/[77]
$RbCsMAFAPbI_{3-x}Br_x$	1.74	IBC	0.16; 4	16.0 + 10.4 = 26.4*	ANU	2017/[78]
$MAPbI_3$ (module)	1.55	IBC	4; 4	12.0 + 8.2 = 20.2	IMEC	2017/[79]

Monolithically integrated two-terminal							
Perovskite	E_g [eV]	Silicon	Recombination layer	Area [cm^2]	PCE [%]	Institute	Year/reference
$MAPbI_3$	1.55	Homojunction	n^{++}/p^{++} Si tunnel	1	13.7	MIT/Stanford	2015/[71]
$FAMAPbI_{3-x}Br_x$	1.56	SHJ	ITO	0.12	18.1*	HZB/EPFL	2015/[80]
$MAPbI_3$	1.55	SHJ	IZO	0.17	21.2*	EPFL/CSEM	2015/[81]
$MAPbI_3$	1.55	SHJ	IZO	1.43	20.5*	EPFL/CSEM	2016/[72]
$MAPbI_3$	1.55	Homojunction	ZTO	1.43	16.0*	EPFL/CSEM	2016/[82]
$CsFAPbI_{3-x}Br_x$	1.63	SHJ	ITO	1	23.6*	Stanford/ASU	2017/[73]
$CsFAPbI_{3-x}Br_x$	1.63	SHJ	nc-Si tunnel	0.25	22.8	EPFL/CSEM	2017/[83]
CsFAPbIBr	1.63	SHJ	nc-Si tunnel	12.93	18.0*	EPFL/CSEM	2017/[83]

20.5% was demonstrated on a 1.4 cm^2 monolithic tandem cell (Figure 4c,d), as compared to the previous monolithic tandem cells demonstrated on sizes <0.3 cm^2.[72]

In the meantime, progress was made on the development of perovskite materials with wider bandgaps containing cesium (Cs) cations, resulting in improved device stability and higher reproducibility.[84] McMeekin et al. then used a Cs–formamidinium (FA) double cation perovskite material to open the bandgap to ≈1.74 eV, the ideal value for a top cell absorber material.[74]

Device stability is a major challenge for the development of perovskite solar cells and particularly for their implementation in tandem solar cells with silicon technologies. Thermal stability is necessary for the cell to survive conventional encapsulation with >100 °C annealing temperature and to pass damp heat testing protocols. Bush et al. demonstrated that perovskite solar cells featuring TCO front and rear electrodes (and thus suitable for tandem integration) show improved thermal stability as compared to cells with a metal rear electrode. The TCO rear electrode acts as an efficient barrier for moisture ingress and prevents the loss of volatile organic compounds from the absorber layer.[85]

In February 2017, the same group managed to pass a 1000 h damp heat test at 85 °C and 85% relative humidity with a semitransparent perovskite solar cell, using an inverted polarity (p-i-n) and a CsFA double cation perovskite material. In the same publication, a 1 cm^2 monolithic tandem with 23.6% efficiency was demonstrated,[73] the current record value for a perovskite/silicon monolithic tandem cell (Figure 4e,f).

The performance of mechanically stacked four-terminal tandem cells also gradually increased, mostly driven by the improved efficiency of single-junction semitransparent perovskite cells. An important progress was made in 2016 with the first experimental demonstration of >25% total efficiency.[72] The latest record is held by Catchpole and co-workers at the Australian National University (ANU), with a 26.4% efficiency obtained from a four-terminal tandem measurement combining a small 0.16 cm^2 top cell with a larger 4 cm^2 back-contacted silicon bottom cell.[78] Until now, most published four-terminal results were based on indirect performance measurements combining a small perovskite top cell (<1 cm^2) with a larger silicon bottom cell. However, first progress in upscaling the perovskite top cell has already been made. 1 cm^2 semitransparent perovskite cells were demonstrated with a 14.5% efficiency.[72,73] When combined into a fully integrated four-terminal tandem device with a silicon heterojunction bottom cell of the same size, an efficiency of 23.2% was reached.[86] Further upscaling typically involves reducing resistive losses in the

transparent electrodes and scribing of the layer stack to define segments and to interconnect them into a module. Semitransparent modules with an aperture area of 4 cm^2 were recently demonstrated, reaching an efficiency of 12%, which led to a module-on-cell four-terminal tandem with 20.2% efficiency.[79]

4. Performance Optimization

As shown above, the performance of perovskite/silicon tandem cells has rapidly improved in recent years. However, the current state-of-the-art efficiency of ≈26%[78] is still well below the radiative limit of 43%. In a tandem solar cell, ideally all photons with energy above the top cell bandgap should be absorbed in the top cell absorber material and all the remaining photons with energies above the bottom cell bandgap should be harvested by the bottom cell. In reality, a significant part of the light can be lost by parasitic absorption in the transparent electrodes, the charge transport layers, the recombination layer, and the metallization. Reflection losses and a nonideal perovskite top cell absorber layer thickness and bandgap lead to a further reduction in tandem cell performance. In this section, we present the developments that enabled the fast progress of this research field and discuss the above-mentioned challenges that still limit performance.

4.1. Low Temperature Planar Perovskite Cells

Developing perovskite-based tandem solar cells necessarily requires an adaptation of the single-junction cell fabrication process and this is particularly true for the monolithic tandem configuration. Historically, perovskite solar cells were first based on the dye-sensitized solar cell architecture, including a TiO_2 mesoporous scaffold layer requiring a sintering step at 500 °C.[70] This relatively high temperature is not of concern for four-terminal tandem cells, where both subcells are fabricated separately. For monolithic tandem cells, however, this process temperature limits the options for the silicon bottom cell to diffused-junction or "tunnel oxide" cells. Silicon heterojunction solar cells, currently the crystalline silicon technology with the highest performance and therefore especially interesting for high-efficiency silicon-based tandems, are only compatible with top cell processes up to ≈200 °C. Above this temperature, the hydrogen from the amorphous silicon layers passivating the wafer surfaces starts effusing, which strongly affects passivation and hence leads to reduced V_{OC}.[3]

After an initial phase, when mesoporous perovskite solar cells were dominating the field, planar, i.e., scaffold-free cells started to catch up, driven by improvements of the perovskite material quality and better interface control.[87] The removal of the scaffold structure enabled the development of highly efficient perovskite cells, which are fully processed at low temperatures (<200 °C) and compatible with silicon heterojunction bottom cells.[72,88–90] Charge transport layers deposited at low temperatures include p-type 2,2′,7,7′- Tetrakis(N,N-di-4-methoxyphenylamino)-9,9′-spirobifluoren (spiro-OMeTAD), poly(3,4-ethylenedioxythiophene)-poly(styrenesulfonate) (PEDOT:PSS), poly(triarylamine) (PTAA), and nikel oxide (NiO_x), as well as n-type TiO_2, SnO_2, C_{60}, and PCBM, among others.[87,91,92]

4.2. Transparent Electrodes

A large part of the initial effort on perovskite/silicon tandem cell development was dedicated to the search for an appropriate transparent electrode as replacement to the opaque metal rear contact normally used in perovskite solar cells. This electrode is a key feature of both two- and four-terminal tandems, and should be highly transparent in a wide spectrum range, including the near-infrared region to maximize the amount of light transmitted to the bottom cell.[93] **Figure 5** presents the main candidates that have been investigated.

Silver nanowire mesh electrodes were demonstrated by several groups, usually deposited by spray coating and mechanical transfer.[69,96,98] Questions about stability were however rapidly raised, due to the formation of silver halide complexes through reaction with ions from the perovskite layer.[85,99] Also, the complexity of the fabrication technique and the low reproducibility might severely limit the application of silver nanowires in larger-scale tandem devices. Graphene oxide fabricated by chemical vapor deposition was shown to have a high transparency, however, with a high sheet resistance of up to 350 Ω sq^{-1}.[100,95] Transparent electrodes based on thin evaporated metal layers were also demonstrated, e.g., Au,[101] MoO_x/Au/MoO_x,[45] and Cu/Au.[76] They have the advantage of process simplicity, however with the disadvantage of strong parasitic absorption, especially in the top cell sub-bandgap spectral range. For example, the Cu/Au bilayer electrode[76] shown in Figure 5g leads to a perovskite top cell sub-bandgap absorption between 20% and 30% in the 800–1200 nm wavelength range where the silicon bottom cell absorbs.

TCOs were already used for early demonstrations of semitransparent perovskite cells, initially based on a sputtered ITO layer.[68] This early test was suffering from suboptimal electrical properties of the as-deposited ITO. The normally required annealing at a temperature >200 °C was not possible due to the temperature sensitivity of the materials used in the perovskite cell. Later, the appropriate replacement was found by the same group with IZO,[70] an amorphous TCO having, without any post-treatment, a high conductivity, a high carrier mobility of >50 cm^2 V^{-1} s^{-1}, and a reasonably low carrier density to limit free-carrier absorption in the infrared spectral region. Other suitable high-mobility TCOs were also reported, including Al-doped ZnO[46] and hydrogenated indium oxide (IO:H).[72] ITO can however also be used, when carefully adjusting deposition conditions and increasing the thickness to compensate for the lower conductance of as-deposited layers.[85]

The performance of four-terminal tandem devices is also sensitive to the TCO used for the top cell front electrode (i.e., the one at the substrate side), commonly fluorinated tin oxide (FTO) or ITO. Even though FTO was adopted by a large majority of the perovskite community, thanks to its high chemical and thermal stability, it is not well suited for tandem applications as it shows high free-carrier absorption in the near-infrared spectral region. The bottom cell current in a four-terminal tandem that employs

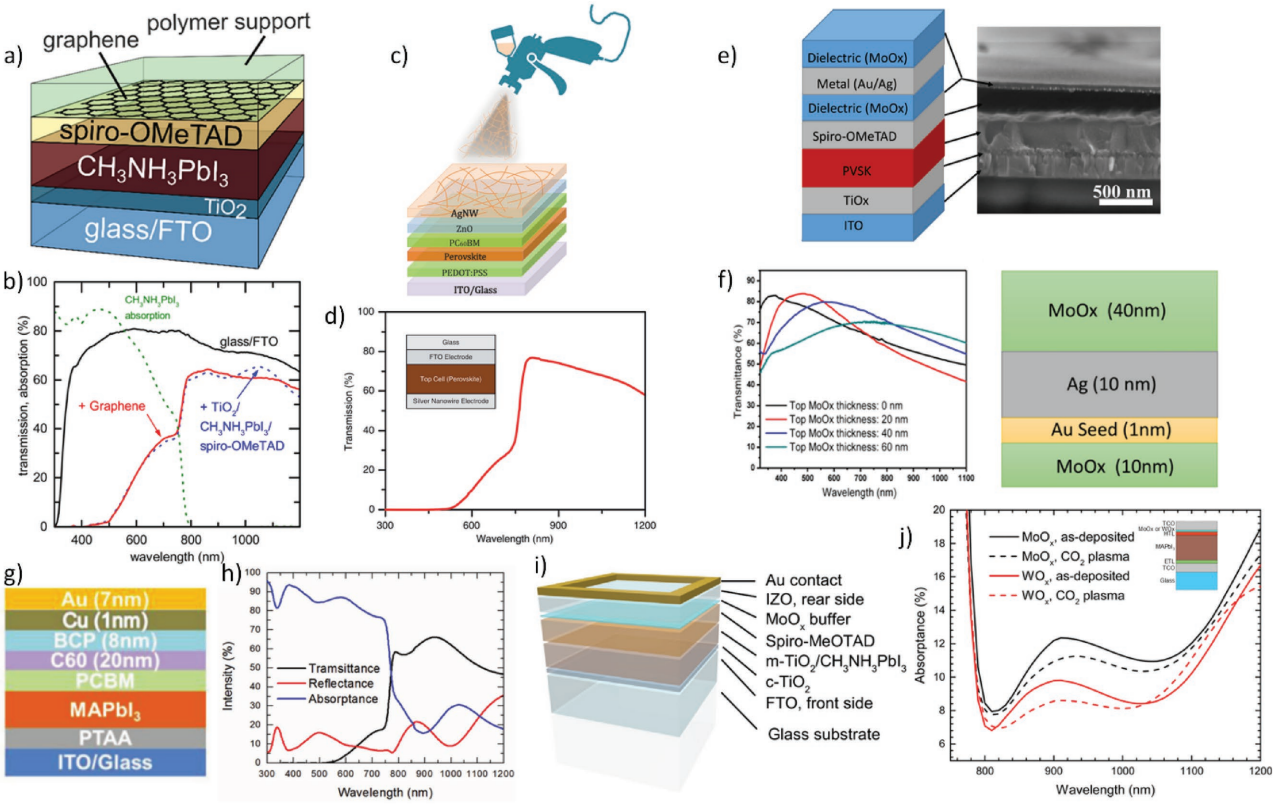

Figure 5. a) Schematic illustration of a semitransparent perovskite solar cell with graphene electrode. Reproduced with permission.[94] b) Transmission spectra of a perovskite cell with graphene transparent electrode. Reproduced with permission.[95] Copyright 2015, American Chemical Society. c) Drawing of a semitransparent perovskite solar cell with spray-deposited Ag nanowire electrode. Reproduced with permission.[96] Copyright 2014, Royal Society of Chemistry. d) Transmission spectrum of a perovskite solar cell with a Ag nanowire electrode mechanically transferred by lamination. Reproduced with permission.[69] Copyright 2014, Royal Society of Chemistry. e) Schematic view and scanning electron microscope image of a perovskite solar cell with a MoO_x/metal/MoO_x multilayer electrode and f) the transmittance spectra of this electrode. Reproduced with permission.[45] Copyright 2015, American Chemical Society. g) Schematic of the layer stack of a semitransparent perovskite solar cell with an electrode composed of thin metal multilayers and h) the spectrophotometric measurements of this cell. Reproduced with permission.[76] i) Device graphical view of a semitransparent perovskite solar cell with IZO as transparent rear electrode and MoO_x as sputtering buffer layer. Reproduced with permission.[70] Copyright 2015, Elsevier. j) Absorptance curves of semitransparent perovskite solar cells with different metal oxide buffer layers. Reproduced with permission.[97] Copyright 2016, American Chemical Society.

a FTO electrode is therefore drastically reduced, as compared to, for example, less absorbing TCO such as ITO.[70,102]

Another drawback of TCO electrodes is that their deposition by sputtering tends to damage sensitive charge transport materials when deposited onto the perovskite top cell layer stack. Therefore, buffer layers have to be introduced between organic charge transport layers (e.g., spiro-OMeTAD in n–i–p cells, or fullerenes in p–i–n cells) and the TCO. Molybdenum oxide (MoO_x), a thermally evaporated transition metal oxide, has typically been used for the p-type contact.[46,68,70,72,81] It was however found to interact with the Ar plasma during the sputter deposition, increasing its absorption due to the increased number of oxygen vacancies.[97] As shown in Figure 5j, a solution to this problem was found by replacing MoO_x with tungsten oxide (WO_x), a more resilient metal oxide. Remarkably, the sub-bandgap absorptance of the whole top cell layer stack was then below 10% between 800 and 1100 nm. For p–i–n cells, where the transparent electrode is deposited on the n-type charge transport layer, several options exist as well: e.g., ZnO nanoparticles[47,85] and SnO_2 thin films grown by atomic layer deposition.[73]

4.3. Parasitic Absorption in Charge Transport Layers

The most commonly used hole transport material, spiro-OMeTAD, shows strong parasitic absorption mainly in the blue and UV spectral region when it is placed in front of the perovskite absorber layer, as in a monolithic tandem cell in the n–i–p configuration (illustrated in **Figure 6**a by the yellow area below 400 nm). This represents a current loss of 1–2 mA cm^{-2}. In the case of four-terminal tandem cells, these losses impose the superstrate configuration for the top cell. Such parasitic losses are strongly limiting the potential efficiency of the tandem device and therefore, this material has to be replaced by a thinner, lowly doped layer with minimal parasitic absorption.[103] Alternative hole transport layers allowing for lower parasitic absorption include thin layers of small-molecule semiconductors, such as N,N'-bis(naphthalen-1-yl)-N,N'-bis(phenyl)-benzidine (NPB), 2,2',7,7'-Tetra(N,N-ditolyl) amino-9,9- spirobifluorene (spiro-TTB), or N4,N4,N400,N400-tetra([1,10- biphenyl]-4-yl)-[1,10:40,100-terphenyl]-4,400-diamine (TaTm),[104,105] as well as the inorganic NiO_x and copper

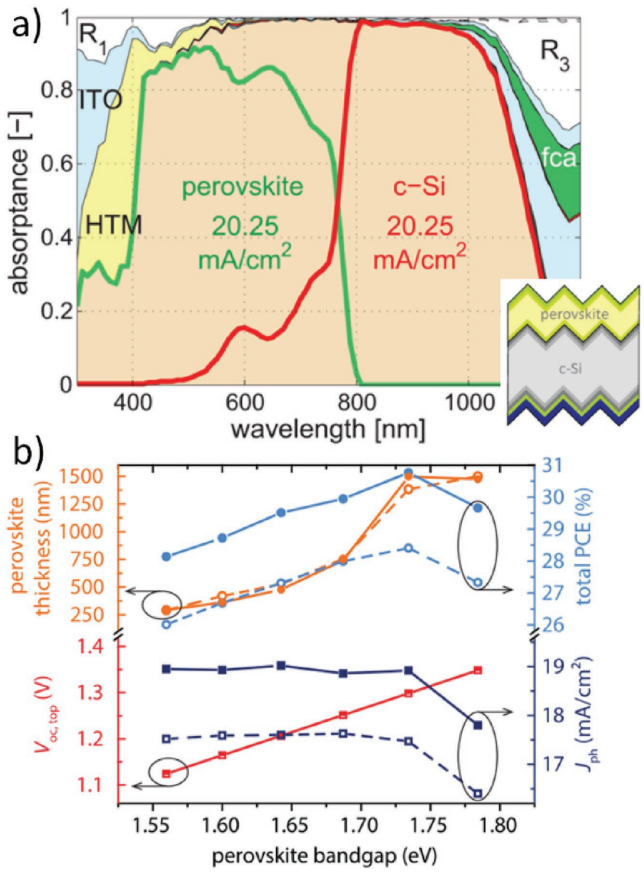

Figure 6. a) Simulated parasitic absorption and reflection losses of a current-matched two-terminal tandem with textured surfaces and conformal top cell deposition. Reproduced with permission.[109] Copyright 2017, Optical Society of America. b) Comparison of monolithic perovskite/silicon tandem cells comprising of a top cell with either the n–i–p (dashed lines) and p–i–n (solid lines) polarity, as function of the top cell bandgap. Reproduced with permission.[110] Copyright 2017, Optical Society of America.

thiocyanate materials with high bandgaps.[106–108] Thin layers of fullerenes, e.g. phenyl-C_{61}-butyric-acid-methyl-ester (PCBM) or buckyball (C_{60}), were shown to be suitable electron transport layer with reduced parasitic absorption, for both the p–i–n[72] and the n–i–p[47,73] configurations.

As a result, the latest performance improvement for monolithic tandem devices can largely be credited to reduced parasitic absorption in the charge transport layers, using a p–i–n configuration with NiO_x and PCBM as hole and electron transport layers, respectively, with the n-type contact facing the sun.[73] This improvement can be directly observed when comparing the extermal quantum efficiency (EQE) spectra in the UV/blue spectral range of monolithic tandem cell either with the n–i–p polarity and spiro-OMeTAD hole transport layer (Figure 4d) or the p–i–n polarity with PCBM electron transport layer (Figure 4f). Dedicated effort will still be required to further reduce parasitic optical losses in the charge transport materials and develop stable organic or inorganic materials with high optical bandgap, which form conformal, dense layers even for small thicknesses, and can be deposited onto the perovskite layer without inducing damage.

4.4. Efficient Wide-Bandgap Perovskite Cells

The most widely used perovskite material composition is MALI with a bandgap of ≈1.55 eV, which is below the optimal value of ≈1.73 eV for an ideal top cell in monolithic tandems with silicon bottom cell. For four-terminal tandem cells, the ideal bandgap is slightly larger, even though high efficiencies can also be reached with nonideal top cell bandgaps due to the considerably less pronounced performance drop for lower bandgaps (see Figure 3). Although, MALI top cells were well suited for initial proof-of-concept tandem devices, demonstrating that efficiencies beyond the single-junction silicon record, especially for monolithic tandems, requires top cells with a ≈0.2 eV higher bandgap. This increase in bandgap has to be reached while still preserving material and interface quality, to obtain a corresponding increase in V_{OC}. The bandgap of methylammonium (MA)-based perovskites can easily be increased by substituting part of the iodine with bromine, yielding values between 1.55 and >2 eV.[111] However, the stability of these compounds has been found to be highly limited, subjected to photoinduced phase segregation and phase separation.[112–115]

A breakthrough concerning phase stability was reached with the introduction of perovskite materials containing the Cs and FA cations, either partially or fully replacing methylammonium.[74,84] For example, using the ($FA_{0.83}Cs_{0.17}Pb(I_{0.6}Br_{0.4})_3$) material that has a bandgap of 1.74 eV, perovskite cells with an efficiency of up to 17% were demonstrated, yielding a V_{OC} of 1.2 V, close to the theoretical potential of 1.42 V.[74] Moreover, Beal et al. showed that the methylammonium cation is volatile and tends to evaporate from the device under thermal stress during device operation, such that replacing it with cesium considerably improves the thermal stability.[116] The purely inorganic $CsPbBrI_2$ material showed a suitable bandgap close to 1.9 eV. However, the cell performance was still very limited due to a nonoptimized deposition process and a too thin absorber layer. The $CsPbI_3$ composition would be highly suitable for tandem applications as well, with a bandgap of 1.73 eV.[117] Unfortunately, its photoactive phase is unstable at room temperature.[118]

Unger et al. compared reported data of perovskite cells with bandgaps between 1.2 and 2.2 eV and found that most reported V_{OC} followed the expected monotonic increase for bandgaps up to ≈1.7 eV. For larger bandgaps, strong deviations were observed, which they attributed to a phase separation, resulting in a lower V_{OC}.[21] Further work will therefore be required to improve the crystallinity and ionic homogeneity in wide-bandgap perovskite materials.

The charge extraction layers must also be adapted to these new compositions with higher bandgaps as shown by Lin et al.[119] Increasing the bandgap typically shifts the conduction band toward higher energies. Thus, adapting the energy levels of the electron transport layer helped to increase the V_{OC} and reach efficiencies as high as 18.5% with a bandgap of 1.71 eV.

Even though the optimal top cell bandgap is 1.73 eV for ideal monolithic tandem cells, current matching can still be reached with bandgaps of 1.6–1.65 eV in state-of-the-art devices, due to the parasitic absorption in the UV–visible spectral part in the transparent front electrode and in the charge transport layers. These devices did not reach ultimate performance, but further

increasing the top cell bandgap will also not be beneficial before the top cell spectral response is increased in that wavelength range. In addition, monolithic tandem cells typically show their highest performance at a slight current mismatch, when the subcell with the higher fill factor is current limiting.[120] Assuming that high-performance silicon bottom cells typically still exhibit higher fill factors, the ideal top cell bandgap might be slightly below the above mentioned ideal values.

4.5. Absorber Thickness and Morphology

An additional factor, which strongly affects the top cell photocurrent is the perovskite absorber layer thickness. Figure 6b shows the optimal perovskite layer thickness in the monolithic configuration depending on the top cell bandgap. For an ideal bandgap of 1.73 eV, the perovskite layer thickness should be ≈1 µm, which is still experimentally challenging while keeping high material quality. Therefore, in practice, a trade-off exists between complete light absorption during the first light pass and effective carrier collection, which requires high electronic quality through the entire film. Electro-optical studies can then be carried out to find the limitations related to a specific perovskite deposition technique.[121]

With lower-bandgap materials, such as those used in the first demonstrations of monolithic tandem cells,[71,80,81] the perovskite thickness could be made thinner, usually around 350 nm, to satisfy the current matching condition. Current matching through absorber thickness optimization will be even more relevant for triple junction solar cells, e.g., using two perovskite absorber layers stacked on a silicon cell.

These calculations assume a fully homogeneous and high-quality perovskite layer. However, the formation of nonuniformities and pinholes during deposition of thick perovskite films can drastically reduce the device performance. The optimization of thin-film deposition processes can be supported by specific characterization techniques, allowing for the detection of these imperfections, further improving the growth conditions and further understanding the influence of microstructure.[122]

Laser beam induced current can be used to map the photocurrent nonuniformities in the individual tandem subcells, when combining appropriate bias light and laser probe wavelengths.[123] This technique was shown to be useful to reveal the effect of, for example, impurities due to nonfiltered solutions used during fabrication by spin coating.

The material quality can be further analyzed by multiwavelength photoluminescence (PL) mapping.[124] PL can show electronic defects in semiconductor materials. As a result, by characterizing the tandem layer stack along the process flow, it is possible to relate processing conditions or substrate surface state with observed defects in specific cell layers. Improving the perovskite absorber layer quality by better understanding its growth mechanism can then be helpful to reduce nonradiative recombination.

Combining PL with electroluminescence allows us to gain further knowledge about the limiting factors of the tandem device: Hyperspectral luminescence imaging of perovskite solar cells can be used to map the photovoltage and charge carrier transport efficiency.[125] For example, areas in the device with a low collection efficiency of photogenerated charge carriers could be related to interfacial resistance fluctuations, leading to low fill factors. Improvement comes then with better interface engineering and energetics consideration when specifically choosing contact materials in function of the absorber material composition.

4.6. Reducing Reflection Losses

High-efficiency silicon single-junction cells use a textured front side to reduce reflectance losses. While this does not cause any issues for four-terminal tandem integration, it is problematic for monolithic tandems as the conformal, pinhole-free deposition of the top cell layers on such textured substrates with many sharp features is challenging. As a result, already the earliest demonstrated four-terminal perovskite/silicon tandem cell used fully textured bottom cells, whereas all monolithic perovskite/silicon tandem cells reported so far use front-side polished silicon wafers. This polished front side leads to reflection losses, originating from the difference in refractive index at the front surface (between the front electrode and air) and the interfaces in the top cell layer stack. This leads to strong interference as exhibited by the EQE spectra shown in Figure 4d,f.[71,73,80,81] When using an intermediate recombination layer based on a TCO, its thickness can strongly affect interference losses.[80–82] It was shown that a minimum thickness of about 20 nm was necessary to reach a correct electrical cell behavior, but slightly thicker layers were beneficial for the overall current generation, mostly affecting the silicon bottom cell spectral response.[81] The optimal thickness was found to be dependent on the type of TCO and on the materials used in the neighboring layers. The reflection due to the intermediate junction can be tuned by adjusting its refractive index, for example, by replacing the TCO ($n \approx 1.8$–2) with oxygen-rich nanocrystalline silicon layers ($1.8 < n < 4$) as already used in thin film silicon tandem solar cells.[126,127] A report under review demonstrates that the use of a nanocrystalline silicon junction in perovskite/silicon monolithic tandem cells, effectively reduces parasitic absorption and reflection losses of red and infrared light, thus helping to increase the current generated in the silicon bottom cell.[83] In mechanically stacked four-terminal tandem devices, the two subcells are physically separated and electrically isolated. However, they must be optically coupled to avoid reflection losses at the interfaces between the subcells and to enhance near-infrared light incoupling into the bottom cell. The coupling material should be transparent, insulating, and have a refractive index close to those of the transparent electrodes used at the interfaces of the subcells. For example, an epoxy resin layer ($n \approx 1.6$) was found to work well for III–V/Si four-terminal tandem.[128]

A further reduction of the reflection losses can be achieved with antireflection coatings, following the quarter wavelength thickness rule. For silicon cells, the front passivation dielectric layer (e.g., SiN_x) or front TCO contact with proper thickness is typically used. For perovskite cells and perovskite-based tandem cells, layers based on LiF,[71,73,80] MgF_2,[16,78] or SiO_2[129] have been used at air/glass and air/TCO interfaces. In the near future, we expect to see more research activity on the specific development of broadband antireflection coatings, as it was previously done for other thin film technologies such as amorphous silicon.[130,131]

Ultimately, depositing the perovskite on front side textured silicon wafers would give the lowest reflection and therefore the highest photogenerated currents, with potential for >20 mA cm^{-2} in each subcells (Figure 6a).[109] This development would therefore represent a major step toward tandem cells beyond the single-junction limit. The antireflective effect of the front side texture, e.g., random pyramids with {111} silicon facets, is obtained by enhancing the probability of the reflected light to bounce back on the surface of the cell. As a result, more light is transmitted into the device.

When front side texturing is practically not feasible directly at the wafer surface, a microtextured foil (texture replicate on a plastic foil) can be applied on the front electrode of the solar cell during its characterization.[132,133] This technique was already used several times for perovskite-based single and tandem cells.[72,78,80,81,129,134–136] An example of the effect of such a microtextured antireflection foil can be seen in Figure 4d.

4.7. Light Trapping

Absorber materials with indirect bandgap, such as crystalline silicon, exhibit weak light absorption near their absorption edge. As a result, light trapping strategies have to be employed to increase the path length toward the theoretical limit given by the Yablonovitch formula of $4n^2$, with n being the refractive index of the absorber material. Texturing both interfaces of the silicon wafer is the most common strategy for crystalline silicon cells. Already a textured rear side helps to trap light in the wafer, which was experimentally shown to increase the bottom cell current by 0.77 mA cm^{-2} in the wavelength range >1000 nm.[72] From simulations and optical modeling, it is clear that a fully textured bottom cell would yield the highest current,[103,109] both by reduced reflection and by light trapping of infrared light in the bottom cell. The light trapping effect in the conformally coated top cell would however rely on a well-designed intermediate contact acting as partial reflector for the short wavelengths and incoupling layer for the wavelengths above the perovskite absorption edge.[137]

5. Toward Market Entry

To be viable for a silicon-based tandem PV product, the perovskite top cell is required to comply with the typical field warranty for PV panels, i.e., the power output should remain >80% after 25–30 years. In addition, tandem cells must be manufactured on industrial-scale wafers (typically 6 in.), with techniques and materials that add limited costs to the final product, which also concerns production throughput and yield. Stability, upscalability, and cost-effectiveness are therefore the three most important keys for a possible commercialization.

5.1. Device Stability

Stability has been a serious concern since the very beginning of the perovskite cell development. In the early 90s, Mitzi et al. did not pursue his work on perovskite materials for photovoltaics exactly because of their poor stability.[60] Later on, the first solar cells with a perovskite absorber were stable for only a couple of minutes, at the time mainly because of the use of a liquid electrolyte.[61] However, in the last five years, tremendous progress was achieved and more and more research groups have shown hundreds to thousands of hours of reliability data according to standardized degradation protocols. We will here only shortly summarize some important improvements in cell design and material properties responsible for this promising progress in cell stability. For more in-depth information on this topic, excellent specific reviews were recently published elsewhere.[138,139]

5.1.1. Perovskite Material Stability

For photovoltaic applications, the perovskite absorber layer must keep its desired crystallographic phase during device operation. The MALI perovskite material displays a tetragonal phase at room temperature but has a phase transition to a cubic phase at a temperature of ≈60 °C,[140] which is in the operational temperature range of a photovoltaic module. The methylammonium cation was also shown to be very volatile, effusing from the cell under thermal stress.[141] Furthermore, increasing the bandgap of MALI by substituting partially the iodide with bromide tends to make the new compound very unstable under light, due to phase segregation.[113] Therefore, it is clear that even though this compound is easy to fabricate and already relatively well understood, it will not be suitable for commercialization. Structural stability improvements were obtained by replacing the methylammonium cation with a larger cation such as FA. $FAPbI_3$ has a cubic ("black") phase at room temperature after annealing at 150 °C, but often with residues of a hexagonal ("yellow") phase. Such additional non-photoactive phases (e.g., hexagonal phase of $FAPbI_3$ or nonconverted PbI_2) can act as seeds for degradation propagation in the film.[142] The current world record for single-junction perovskite solar cells was obtained with a FA–MA mixed-cation and I–Br mixed halide material, with a certified efficiency of up to 22.1%,[14] and improved stability at room temperature. Thermal stability of this composition is however still a concern. An important progress in material stability came with the introduction of inorganic cations: cesium[84,116,143,144] and later rubidium.[16,17,78,145] In combination with MA and/or FA, they have been shown to drastically improve the structural stability of the perovskite material. Cells containing cesium and rubidium cations retained 95% initial performance after hundreds of hours of maximum power point tracking.[17]

Currently, $CsFAPbBr_xI_{3-x}$ perovskite materials seem to be the most promising high-performance option to reach sufficient thermal stability, showing resistance to annealing temperatures of up to 130 °C without degradation,[74,85] Fully inorganic Cs-based perovskite materials even show significantly higher temperature stability, although at still very limited device performance.[116]

In addition, compared to $MAPbI_3$,[146,147] $CsFAPbBr_xI_{3-x}$ layers showed strongly improved resistance to photo-oxidation and moisture-induced degradation.[148,149] An improved environmental stability of the absorber material can help to lower the constraints on the device encapsulation, and potential related extra costs.

5.1.2. Charge Transport Layers and Electrodes

Apart from the degradation pathways related to the perovskite material, the stability of the charge transport layers present on both sides of the absorber layer is also crucial. Dopants and additives such as 4-tert-butylpridine in spiro-OMeTAD were shown to corrode $MAPbI_3$ and degrade it to PbI_2.[150] Spiro-OMeTAD itself tends to crystallize upon annealing, deteriorating its contact to the perovskite layer.[151] ZnO is known to react with perovskite during annealing or under illumination, attributed to its basic surface favoring the deprotonation of methylammonium cations.[152]

For single-junction perovskite cells, an opaque metal rear electrode is typically used. However, several groups have reported that this metal layer can be the source of degradation either by corrosive reactions with by-products of the perovskite absorber degradation (hydroiodide, methylammonium iodide (MAI)), by redox reactions between the metal electrode and the perovskite absorber material[153] or by migration of metal particles into the organic charge transport layer.[99,154,155] Different metals were tested (Au, Ag, Cu, Al) upon thermal and illumination stress, in all cases resulting in a strong decay in cell performance. To mitigate these interactions, buffer layers were proposed, such as Cr[154] or MoO_x.[155] Even though they allow for an apparent stability improvement, it is not clear if these degradation pathways were fully eliminated or simply slowed down. Due to these various interactions, metals should be avoided as well in transparent electrodes for tandem applications, such as thin metal films or metal/dielectric multilayers.[45,76]

Alternatively, as described above, TCOs are highly suitable for transparent electrodes in perovskite/silicon tandem cells. They do not only provide a high transparency and sufficient lateral conductivity, but also have been shown to be chemically stable against reactions with many materials and possible degradation by-products present in the underlying layers, including charge transport layers and the perovskite absorber. Finally, TCOs also act as an effective barrier for both incoming and outgoing elements: water and oxygen are kept away and the possibly volatile ions in the perovskite material are kept inside the cell.[85]

For sputtered TCO electrodes, buffer layers are however necessary to protect sensitive layers underneath. For the hole-extraction contact, MoO_x was demonstrated as a suitable buffer material.[70] However, stability concerns have been raised due to a possible reaction with the perovskite material[156] and due to the intrinsic environmental sensitivity of many evaporated metal oxides.[97] For the electron-extraction contact, aluminum-doped zinc oxide (AZO) nanoparticles were demonstrated as effective sputtering buffer,[85] but again stability can be an issue due to corrosive interface reactions.[139] SnO_2 grown by ALD can act as an n-type sputtering buffer layer[73] and as a gas permeation and moisture ingress barrier.[157,158]

Further work will be required to confirm that such electrodes are completely inert toward reactions with all materials used in the cell in the long term, i.e., proving that it will retain its properties over the entire lifespan of the photovoltaic module.

5.1.3. Encapsulation, Metallization, and Reliability Testing

The development of an appropriate encapsulation scheme for perovskite single-junction solar cells can rely on decades of research and development for thin-film photovoltaics and optoelectronic applications, such as organic light emitting diodes and flat panel displays. However, in the particular case of perovskite/silicon tandem solar cells, the standards already in place in the silicon PV industry have to be adopted to enable market entry and faster acceptance by a highly conservative industry. Reliable encapsulation schemes, e.g., a glass/glass encapsulation using a polymer encapsulant and a butyl rubber or polyisobutylene[159] edge sealant require a thermal stability of at least ≈120–160 °C, depending on the encapsulation material used. A thermal stability in this range will also allow for the use of industrially viable metallization using screen printing of low-temperature silver pastes. As an additional requirement for market entry, perovskite/silicon tandem cells will have to pass reliability protocols according to the International Electrotechnical Commission (IEC) standards, including damp heat at 85 °C/85% relative humidity, thermal cycling, and extended light soaking tests at 1 sun illumination. The complete IEC standards can be found elsewhere.[160]

McGehee and co-workers have developed semitransparent perovskite solar cells with a $CsFAPbBr_xI_{3-x}$ absorber layer.[73] With this thermally stable material, an effective moisture barrier created by the SnO_2/ITO electrode and an ethylene vinyl acetate (EVA) glass/glass encapsulation, they could pass damp heat testing for 1000 h at 85 °C/85% relative humidity, with minimal degradation, as shown in **Figure 7**. Although not all cells systematically passed the test, this proof-of-concept is very encouraging and promising for the commercialization of perovskite/silicon tandem solar cells. In addition, Oxford PV, a start-up company aiming to commercialize perovskite/silicon tandem cells, announced tandem cells that passed standardized

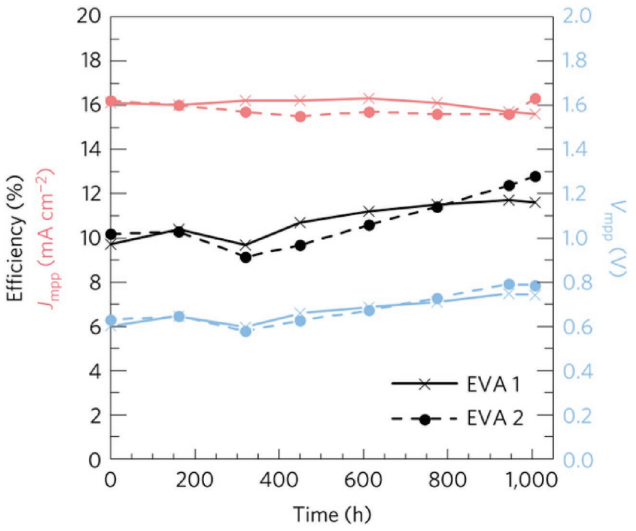

Figure 7. Damp heat test (85 °C/85% relative humidity) of a semitransparent perovskite solar cell with EVA glass–glass encapsulation and butyl edge sealing. Reproduced with permission.[73] Copyright 2017, Nature Publishing Group.

damp heat, thermal cycling, and light soaking reliability tests.[161]

It should be noted that IEC tests only provide an indication of the chance of products to survive in the field. However, as long as the exact degradation mechanisms and the activation energies of theses mechanisms are neither known nor understood, it cannot be assumed that IEC tests are sufficient.

5.2. Device Area Upscaling

Most perovskite solar cells, including the devices with record efficiencies,[14,17] have been demonstrated on small active areas of typically <0.3 cm^2. A first upscaling step for perovskite cells to 1 cm^2 area already necessitates dedicated work to carefully control film uniformity and reduce pinhole density. Chen et al. demonstrated one of the first 1 cm^2 perovskite solar cell with certified efficiency of 15% using a planar architecture.[162] They showed that by using a heavily doped NiMgLiO inorganic hole transport layer with only 10–20 nm thickness, the shunt resistance of larger cells can be greatly reduced. This may be attributed to a lower pinhole density and less structural defects over the full device area. For mesoscopic cells, improving the perovskite layer quality was found to be the key for high efficiencies on larger cell areas. Li et al. developed a vacuum-assisted solution process to fabricate smooth and uniform perovskite layers.[163] They could demonstrate 20.5% efficiency (19.6% certified), with high uniformity of current generation over the 1 cm^2 cell area, as shown in **Figure 8**a. Tan et al. recently also improved low temperature planar perovskite cells, filling the performance gap with the high-temperature mesoscopic cells by showing 20.3% efficiency on 1 cm^2 area (19.5% certified).[18] Here, reducing interface recombination on the TiO_2 layer was reached by chlorination. This low-temperature method is particularly interesting for tandem applications.

Further upscaling requires different approaches, depending on the application. A perovskite single-junction or top cell for a four-terminal tandem with silicon bottom cell will be fabricated in the form of a thin-film module made by monolithically interconnected segments. Laser-scribing techniques have recently been adapted for segment definition and interconnection in perovskite modules, leading to a rapid decrease in dead area, boosting aperture area efficiency.[165–167]

The optoelectronic properties of the transparent front and rear electrodes determine the optimal segment width and number, and therefore the total V_{OC} achievable for a certain module size. Compromising between optimal electrical and optical performance is then necessary to produce efficient semitransparent perovskite top modules for tandems. A first demonstration of a 4 cm^2 area semitransparent perovskite module yielded a mechanically stacked four-terminal tandem with total efficiency of 20.2%, resulting from the sum of 12% from the perovskite module and 8.2% from an interdigitated back contact (IBC) silicon bottom cell (Figure 8b).[79] The record efficiency for opaque perovskite modules is currently at 16.4% on 4 cm^2 area.[168] While such relatively small perovskite modules can still be deposited by spin coating, further upscaling to industrial module sizes will require fully scalable deposition techniques with considerably reduced material waste. A variety of large-area deposition methods has already been presented for perovskite module fabrication, such as slot-die coating, inkjet printing, blade coating, screen printing, and spray coating. With industrial-scale printing techniques, an efficiency of 11.2% was obtained for a 10×10 cm^2 module, with outdoor stability of over a year.[164,169]

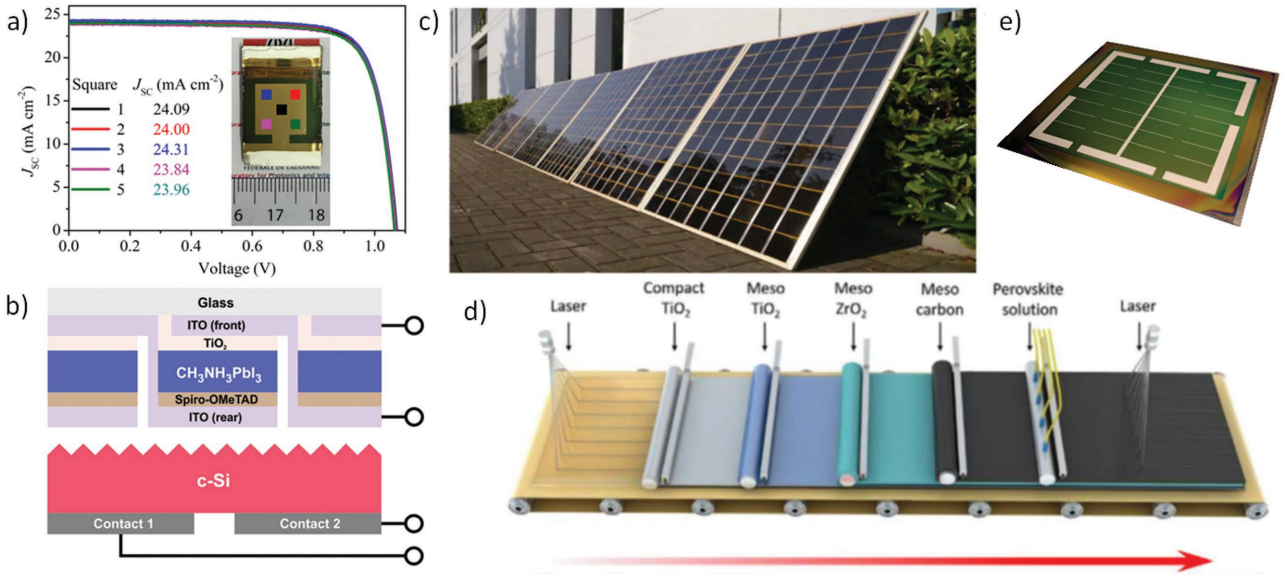

Figure 8. a) *JV* measurement of a perovskite solar cell made by a vacuum-assisted process, with five measurement spots of 0.16 cm^2 on a 1.2×1.2 cm^2 cell. Reproduced with permission.[163] Copyright 2016, AAAS. b) Schematic view of a module-on-cell mechanically stacked four-terminal tandem with a monolithically interconnected semitransparent perovskite module and an IBC silicon bottom cell. Reproduced with permission.[79] c) Example of a large sized perovskite module made with an assembly of smaller 10×10 cm^2 modules and d) the corresponding proposed in-line process flow. Reproduced with permission.[164] e) Monolithic tandem with 12.9 cm^2 aperture area with 18% efficiency.[83]

Reaching module sizes in the m^2 range is still very challenging and large perovskite modules were so far only demonstrated by connecting smaller 10×10 cm^2 mini modules together, as shown in Figure 8c. Potential production processes for opaque perovskite modules were, for example, presented in refs. [164] and [170].

The development of monolithic two-terminal tandems so far mostly focused on aperture areas between 0.16 and 1.4 cm^2.[71,80,81,72,73] Upscaling of this tandem configuration to an industrial level requires different adaptations as compared to single-junction perovskite cells or four-terminal tandems. This is mostly because two-terminal tandem modules consist of wafer-size cells placed next to each other and interconnected by metal ribbons, and not of a single module-size substrate with interconnected segments. As a result, cell upscaling is limited to the current industrial silicon cell size of 6 in. However, additional requirements exist due to cost constraints, as the use of mechanically polished wafers, typically used for most monolithic perovskite/silicon tandem cells so far, is not an option. Scalable fabrication techniques that enable processing the perovskite top cell on fully textured wafers typically used in industry are thus required, such as sputtering, plasma-enhanced or low-pressure chemical vapor deposition, electrodeposition, or thermal evaporation, which was so far less relevant for the silicon PV industry but used, e.g., for organic LED manufacturing. In addition, to enable the integration of the technology in a silicon PV production line, a high throughput (≈1 wafer per 1.5 s) and high yield (≈98%) have to be targeted.

Low-temperature planar perovskite cells currently seem to be the most suitable option for two-terminal tandem upscaling, as they are compatible with silicon heterojunction bottom cells and can readily be made in either polarity, making them suitable for both n- and p-type silicon bottom cell technologies.[80,81] For this device architecture, the perovskite layer can be deposited by thermal coevaporation of the precursors,[104,171] e.g., PbI_2, PbBr, CsI, MAI, FAI, or FABr. This approach is however still challenging, due to the difficulty of controlling accurately the evaporation rates of materials with significantly different volatility. A two-step interdiffusion technique might have advantages considering the integration in an in-line process, because the complex perovskite material formation can be separated in dedicated process steps: the lead halide compound can be thermally evaporated and then converted to the perovskite material by reaction with the organohalide precursors in the gas phase, using a chemical vapor deposition method.[29,172,173]

Finally, series resistance losses in monolithic tandems might be less challenging to mitigate compared to a single-junction thin-film module. The front contact can be made of a TCO and metallization, ultimately by screen printing or electroplating as used in silicon heterojunction solar cells.[174] Internal interfacial resistances are here a major challenge, which requires further intense research.

First demonstrations of upscaled two-terminal perovskite/silicon heterojunction tandem cells were recently presented, with 18% efficiency for 12.9 cm^2 aperture area (Figure 8e).[83] In addition, Oxford PV recently announced the production of 6 in. tandem cells in their new facilities in Germany.

5.3. Material Toxicity and Life Cycle Assessment

Concerns about perovskite material toxicity, and particularly of the Pb content, have been raised.[175] The silicon PV industry is moving to lead-free soldering, which is expected to gradually become the leading technology for interconnections over the next decade.[2] The industrial development of perovskite/silicon tandem cells can therefore be expected to also follow this trend and anticipate future moree strict regulations. Research toward lead-free, or lead-less perovskite solar cells has therefore already started, although device efficiencies still lie far behind those of state-of-the-art lead-containing compounds.[176,177] In parallel, life cycle assessments of perovskite/silicon tandem solar cells[25] and perovskite modules[26] were conducted to define the critical aspects of the currently used materials and processes. It was found that the impact of the use of toxic solvents such as dimethylformamide or dimethyl sulfoxide can have a larger environmental impact than the lead contained in the perovskite absorber layer. Also, the environmental impact of the technology largely depends on its lifetime. Improving the stability of perovskite cells is therefore the key for reducing the overall environmental impact. In addition, an effective encapsulation that retains all degradation by-products is crucial.[175]

5.4. Technoeconomic Considerations

Several studies have addressed the economics of perovskite solar cells.[170,178,179] In this section, we focus on monolithic two-terminal tandem cells, guided by simple considerations of manufacturing processes in production lines, keeping in mind that no fully defined industrial manufacturing process for perovskite-based cells exists yet. For this analysis, we consider the number of process steps required in addition to those for the silicon bottom cell (which could be Al-back surface field (BSF), passivated emitter rear contact (PERC), or heterojunction solar cells). In particular, metallization costs of the front are not included, being already part of the silicon cells. Each process step specific to the perovskite top cell has related investments, costs of consumables, and operational costs (personal, facilities, and maintenance). In **Table 2**, we assume that each process step has related investment costs in the range of 1–3 million euros, allowing for the processing of 3000 wafers per hour or an equivalent of around 400 000 m^2 of panels per year. We make an assumption of 15% operational cost per year compared to investments, and of 1.5 € m^{-2} of consumables per step. The proposed values are in the range of what is possible either for coatings on c-Si wafers (e.g., SiN layer, or ultrathin ALD films), or for thin film processes with low-cost materials (e.g., thin semiconductor layer, 70–100 nm TCO layer). Table 2 shows that, for instance, a 4% absolute efficiency increase, equal to the power output of an additional 40 W m^{-2}, would result in manufacturing costs of 26 €cts per additional watt of output power of the module in the case of four extra process steps, with 1.5 M€ investment per step. A similar cost can also be achieved with more steps, which would however require a higher increase in efficiency.

This represents a good target value, considering the roadmap of c-Si module costs, which are expected to reach

Table 2. Guideline for estimating potential manufacturing costs of the perovskite top cell in a monolithic perovskite/silicon tandem cell. We consider only the extra steps induced by the perovskite top cell deposition (and not the potential steps saved on the c-Si cell). The equipment is depreciated over seven years. Consumable costs of 1.5 € m^{-2} per step and 15% operational costs per year as fraction of CAPEX (capital expenditure, including facilities, maintenance personals) are assumed. For the area related costs savings, 18% nominal module efficiency is considered.

Number of extra steps	Investment (M€ per step)	Depreciation [€ m^{-2}]	Consumables [€ m^{-2}]	Operational costs [€ m^{-2}]	Total process costs [€ m^{-2}]	Absolute efficiency gain [%]	Manufacturing costs [€cts W^{-1}]	Area related BOS cost saving [€cts Wp^{-1}] parks	Area related BOS cost saving [€cts Wp^{-1}] roof top
3	1.5	1.61	4.5	1.69	7.79	4	19.5	2.7	6.4
4	1.5	2.14	6	2.25	10.39	4	26.0	2.7	6.4
5	1.5	2.68	7.5	2.81	12.99	4	32.5	2.7	6.4
3	3	3.21	4.5	3.38	11.09	4	27.7	2.7	6.4
4	3	4.29	6	4.5	14.79	4	37.0	2.7	6.4
5	3	5.36	7.5	5.63	18.48	4	46.2	2.7	6.4
4	2	2.86	6	3	11.86	3	39.5	2.1	5.0
4	2	2.86	6	3	11.86	5	23.7	3.3	7.6

25–30 €cts W^{-1} within the next five to ten years.[180] It is also possible to make a rough estimation of the value related to the enhanced module efficiency. Assuming that the area-related costs are in the range of 27 € m^{-2} for solar parks (all costs excluding inverter) and 63 € m^{-2} for small rooftop systems, the efficiency gain translates into a saving in a range of a few cents (here 2.1–2.7 €cts W^{-1} for solar parks and 6.4–7.6 €cts W^{-1} for rooftops). These values show that even though it will be challenging to reach considerably lower module production costs per watt compared to single-junction c-Si in the mid-term, perovskite/silicon tandem PV systems could be cost competitive as a result of their higher performance, especially for applications where surface area is limited. Then, the higher the efficiency gain, the more BOS cost saved.

The final production costs will include other possible positive factors (reduced costs of metallization, thanks to the high-voltage, low-current device), and potentially also negative ones such as yield (possibility of shunting the top cell) or the requirement for edge sealants in modules. Similarly, the energy yield might be favored by the good temperature coefficient of the top cell, whereas spectral mismatch effects, long-term degradation, and bankability (meaning higher cost of capital) might penalize the cost of electricity produced by such modules.

As a general guideline, in addition to demonstrating real long-term stability, the viability is ensured by two important factors: the increased efficiency gain compared to the original single-junction solar cells, and the reduction of the number of additional process steps (or of the costs associated with each step). Finally, this simple calculation also shows that all usage of expensive material (typically >10 € m^{-2}) will likely prevent any market penetration of this technology.

6. Conclusion and Outlook

Perovskite/silicon tandem cells offer a promising path toward low-cost photovoltaic electricity, by boosting the performance of established crystalline silicon cells at moderate additional production costs. The perovskite research field has massively grown over the last few years and tremendous progress has been achieved on both single-junction and tandem solar cells. In this review, we gave a broad overview on the progress made during this exciting time, while specifically emphasizing on the perovskite/silicon tandem cell development.

Thanks to the small number of layers, enabling low production costs, high efficiency potential with limited parasitic absorption, and their simple implementation at the PV system level, the monolithic two-terminal tandem cell is arguably the most promising and industrially relevant tandem configuration. To further improve monolithic perovskite/silicon tandem cells, effort should be dedicated to the development of conformal deposition processes for fully textured silicon wafers. At the same time, these processes should be compatible with industrial standards and scalable to 6 in. wafers, while keeping the costs as low as possible (<<10 € m^{-2} per layer). In addition, long-term operational stability is an absolute requirement for the commercialization of perovskite/silicon tandem cells, which should reach the same level of reliability as commercially available c-Si solar cells. In order to fully assess and compare the reliability of tandem cells, degradation tests should be first performed according to standardized IEC protocols and possibly then according to adapted protocols, depending on the identified degradation mechanisms.

Marriage of convenience or true love story? Perovskite solar cells clearly have the potential to be an excellent partner for crystalline silicon cells. However, as in any marriage, hard and dedicated work on the remaining challenges will be necessary to make this union a full success. It is not yet possible to give a precise prediction about when the first 30% perovskite/silicon tandem cell will be demonstrated. However, based on the current state-of-the-art and the rapid recent progress, we believe that this challenging target is practically achievable for both the two- and four-terminal tandem configurations. In any case, it is clear that perovskites will continue to surprise us in the coming months and years.

Acknowledgements

The authors would like to thank Dr. Chien-Jen Yang for proofreading. This work was funded by the Nano-Tera.ch "Synergy" project, the Swiss Federal Office of Energy under Grant SI/501072-01, and the Swiss

National Science Foundation via the NRP70 "Energy Turnaround" project "PV2050."

Conflict of Interest

The authors declare no conflict of interest.

Keywords

four-terminal tandem, monolithic tandem, perovskites, silicon heterojunctions

Received: June 22, 2017
Revised: July 26, 2017
Published online: September 11, 2017

[1] World Economic Forum, *Renewable Infrastructure Investment Handbook: A Guide for Institutional Investors*, http://www3.weforum.org/docs/WEF_Renewable_Infrastructure_Investment_Handbook.pdf (accessed: June 2016).
[2] ITRPV, *International Technology Roadmap for Photovoltaic—2016 Results*, http://www3.weforum.org/docs/WEF_Renewable_Infrastructure_Investment_Handbook.pdf (accessed: June 2017).
[3] C. Battaglia, A. Cuevas, S. De Wolf, *Energy Environ. Sci.* **2016**, *9*, 1552.
[4] F. Fertig, R. Lantzsch, A. Mohr, M. Schaper, M. Bartzsch, D. Wissen, F. Kersten, A. Mette, S. Peters, A. Eidner, J. Cieslak, K. Duncker, M. Junghänel, E. Jarzembowski, M. Kauert, D. Meißner, B. Reiche, S. Geißler, S. Hörnlein, C. Klenke, L. Niebergall, A. Schönmann, A. Weihrauch, F. Stenzel, A. Hofmann, T. Rudolph, A. Schwabedissen, M. Gundermann, M. Fischer, J. W. Müller, D. J. W. Jeong, in *7th Int. Conf. on Silicon Photovoltaics*, *SiliconPV*, Freiburg, Germany, **2017**.
[5] SunPower, *X-Series Residential Solar Panels SunPower Residential Solar Panels Engineered for Peace of Mind X-Series*, https://us.sunpower.com/sites/sunpower/files/media-library/data-sheets/ds-x22-series-360-residential-solar-panels.pdf (accessed: June 2016).
[6] K. Yoshikawa, W. Yoshida, T. Irie, H. Kawasaki, K. Konishi, H. Ishibashi, T. Asatani, D. Adachi, M. Kanematsu, H. Uzu, K. Yamamoto, *Sol. Energy Mater. Sol. Cells* **2017**, https://doi.org/10.1016/j.solmat.2017.06.24.
[7] K. Yoshikawa, H. Kawasaki, W. Yoshida, T. Irie, K. Konishi, K. Nakano, T. Uto, D. Adachi, M. Kanematsu, H. Uzu, K. Yamamoto, *Nat. Energy* **2017**, *2*, 17032.
[8] A. Richter, M. Hermle, S. W. Glunz, *IEEE J. Photovoltaics* **2013**, *3*, 1184.
[9] L. C. Hirst, N. J. Ekins-Daukes, *Prog. Photovoltaics* **2011**, *19*, 286.
[10] M. Taguchi, A. Yano, S. Tohoda, K. Matsuyama, Y. Nakamura, T. Nishiwaki, K. Fujita, E. Maruyama, *IEEE J. Photovoltaics* **2014**, *4*, 96.
[11] S. Essig, C. Allebé, T. Remo, J. F. Geisz, M. A. Steiner, K. Horowitz, L. Barraud, J. S. Ward, M. Schnabel, A. Descoeudres, D. L. Young, M. Woodhouse, M. Despeisse, C. Ballif, A. Tamboli, *Nat. Energy* **2017**, https://doi.org/10.1038/nenergy.2017.144.
[12] M. A. Green, A. W.-Y. Ho-Baillie, *ACS Energy Lett.* **2017**, *2*, 822.
[13] J.-P. Correa-Baena, A. Abate, M. Saliba, W. Tress, T. Jesper Jacobsson, M. Grätzel, A. Hagfeldt, *Energy Environ. Sci.* **2017**, *10*, 710.
[14] NREL Efficiency Chart **2017**, http://www.nrel.gov/ncpv/images/efficiency_chart.jpg (accessed: July 2017).
[15] S. S. Shin, E. J. Yeom, W. S. Yang, S. Hur, M. G. Kim, J. Im, J. Seo, J. H. Noh, S. Il Seok, *Science* **2017**, *356*, 167.
[16] M. Zhang, J. S. Yun, Q. Ma, J. Zheng, C.-F. J. Lau, X. Deng, J. Kim, D. Kim, J. Seidel, M. A. Green, S. Huang, A. W.-Y. Ho-Baillie, *ACS Energy Lett.* **2017**, *2*, 438.
[17] M. Saliba, T. Matsui, K. Domanski, J.-Y. Seo, A. Ummadisingu, S. M. Zakeeruddin, J.-P. Correa-Baena, W. R. Tress, A. Abate, A. Hagfeldt, M. Gratzel, *Science* **2016**, *354*, 206.
[18] H. Tan, A. Jain, O. Voznyy, X. Lan, F. P. García de Arquer, J. Z. Fan, R. Quintero-Bermudez, M. Yuan, B. Zhang, Y. Zhao, F. Fan, P. Li, L. N. Quan, Y. Zhao, Z.-H. Lu, Z. Yang, S. Hoogland, E. H. Sargent, *Science* **2017**, *355*, 722.
[19] K. T. Cho, S. Paek, G. Grancini, C. Roldán Carmona, P. Gao, Y. H. Lee, M. K. Nazeeruddin, *Energy Environ. Sci.* **2017**, *2*, 621.
[20] S. De Wolf, J. Holovsky, S.-J. Moon, P. Löper, B. Niesen, M. Ledinsky, F.-J. Haug, J.-H. Yum, C. Ballif, *J. Phys. Chem. Lett.* **2014**, *5*, 1035.
[21] E. L. Unger, L. Kegelmann, K. Suchan, D. Sörell, L. Korte, S. Albrecht, *J. Mater. Chem. A* **2017**, *5*, 11401.
[22] W. Tress, *Adv. Energy Mater.* **2017**, *7*, 1602358.
[23] S. D. Stranks, G. E. Eperon, G. Grancini, C. Menelaou, M. J. P. Alcocer, T. Leijtens, L. M. Herz, A. Petrozza, H. J. Snaith, *Science* **2013**, *342*, 341.
[24] L. M. Pazos-Outón, M. Szumilo, R. Lamboll, J. M. Richter, M. Crespo-quesada, M. Abdi-Jalebi, H. J. Beeson, M. Vrucinic, M. Alsari, H. J. Snaith, B. Ehrler, R. H. Friend, F. Deschler, *Science* **2016**, *351*, 1430.
[25] M. Monteiro Lunardi, A. Wing Yi Ho-Baillie, J. P. Alvarez-Gaitan, S. Moore, R. Corkish, *Prog. Photovoltaics* **2017**, *25*, 679.
[26] I. Celik, Z. Song, A. J. Cimaroli, Y. Yan, M. J. Heben, D. Apul, *Sol. Energy Mater. Sol. Cells* **2016**, *156*, 157.
[27] S. T. Williams, A. Rajagopal, C. C. Chueh, A. K. Y. Jen, *J. Phys. Chem. Lett.* **2016**, *7*, 811.
[28] D. Forgács, L. Gil-Escrig, D. Pérez-Del-Rey, C. Momblona, J. Werner, B. Niesen, C. Ballif, M. Sessolo, H. J. Bolink, *Adv. Energy Mater.* **2017**, *7*, 1602121.
[29] M. R. Leyden, Y. Jiang, Y. Qi, *J. Mater. Chem. A* **2016**, *4*, 13125.
[30] B. Chen, X. Zheng, Y. Bai, N. P. Padture, J. Huang, *Adv. Energy Mater.* **2017**, *7*, 1602400.
[31] N. N. Lal, Y. Dkhissi, W. Li, Q. Hou, Y. B. Cheng, U. Bach, *Adv. Energy Mater.* **2017**, *7*, 1602761.
[32] I. Almansouri, A. Ho-Baillie, S. P. Bremner, M. A. Green, *IEEE J. Photovoltaics* **2015**, *5*, 968.
[33] A. L. Lentine, G. N. Nielson, M. Okandan, J. L. Cruz-Campa, A. Tauke-Pedretti, *IEEE J. Photovoltaics* **2014**, *4*, 1593.
[34] R. Strandberg, in *Proc. of the 42nd IEEE Photovoltaic Specialist Conf.*, IEEE, New Orleans, USA, **2015**.
[35] H. Uzu, M. Ichikawa, M. Hino, K. Nakano, T. Meguro, J. L. Hernández, S. Kim, N. Park, K. Yamamoto, *Appl. Phys. Lett.* **2015**, *106*, 13506.
[36] K. Yamamoto, D. Adachi, H. Uzu, M. Ichikawa, T. Terashita, T. Meguro, N. Nakanishi, M. Yoshimi, J. L. Hernández, *Jpn. J. Appl. Phys.* **2015**, *15*, 08KD15.
[37] R. Sheng, A. W. Y. Ho-Baillie, S. Huang, M. Keevers, X. Hao, L. Jiang, Y.-B. Cheng, M. a. Green, *J. Phys. Chem. Lett.* **2015**, *6*, 3931.
[38] Y. Li, H. Hu, B. Chen, T. Salim, J. Zhang, J. Ding, N. Yuan, Y. M. Lam, *J. Mater. Chem. C* **2017**, *5*, 134.
[39] Z. J. Yu, K. C. Fisher, B. M. Wheelwright, R. P. Angel, Z. C. Holman, *IEEE J. Photovoltaics* **2015**, *5*, 1.
[40] Z. (Jason) Yu, M. Leilaeioun, Z. Holman, *Nat. Energy* **2016**, *1*, 16137.
[41] T. P. White, N. N. Lal, K. R. Catchpole, *IEEE J. Photovoltaics* **2014**, *4*, 208.

[42] N. N. Lal, T. P. White, K. R. Catchpole, *IEEE J. Photovoltaics* **2014**, *4*, 1380.
[43] I. Almansouri, A. Ho-Baillie, M. A. Green, *Jpn. J. Appl. Phys.* **2015**, *54*, 08KD04.
[44] L. Kranz, A. Abate, T. Feurer, F. Fu, E. Avancini, J. Loeckinger, P. Reinhard, S. M. Zakeeruddin, M. Grätzel, S. Buecheler, A. N. Tiwari, *J. Phys. Chem. Lett.* **2015**, *6*, 2676.
[45] Y. M. Yang, Q. Chen, Y.-T. Hsieh, T.-B. Song, N. De Marco, H. Zhou, Y. Yang, *ACS Nano* **2015**, *9*, 7714.
[46] F. Fu, T. Feurer, T. Jäger, E. Avancini, B. Bissig, S. Yoon, S. Buecheler, A. N. Tiwari, *Nat. Commun.* **2015**, *6*, 8932.
[47] F. Fu, T. Feurer, T. P. Weiss, S. Pisoni, E. Avancini, C. Andres, S. Buecheler, A. N. Tiwari, *Nat. Energy* **2016**, *2*, 16190.
[48] S. Pisoni, F. Fu, T. Feurer, M. Makha, B. Bissig, S. Nishiwaki, A. Tiwari, S. Buecheler, *J. Mater. Chem. A* **2017**, *5*, 13639.
[49] T. Todorov, T. Gershon, O. Gunawan, Y. S. Lee, C. Sturdevant, L.-Y. Chang, S. Guha, *Adv. Energy Mater.* **2015**, *5*, 1500799.
[50] T. Todorov, T. Gershon, O. Gunawan, C. Sturdevant, S. Guha, *Appl. Phys. Lett.* **2014**, *105*, 173902.
[51] Y. Liu, L. A. Renna, M. Bag, Z. A. Page, P. Y. Kim, J. Choi, T. Emrick, D. Venkataraman, T. P. Russell, *ACS Appl. Mater. Interfaces* **2016**, *8*, 7070.
[52] J. H. Heo, S. H. Im, *Adv. Mater.* **2015**, *28*, 5121.
[53] F. Jiang, T. Liu, B. Luo, J. Tong, F. Qin, S. Xiong, Z. Li, Y. Zhou, *J. Mater. Chem. A* **2016**, *4*, 1208.
[54] M. Anaya, J. P. Correa-Baena, G. Lozano, M. Saliba, P. Anguita, B. Roose, A. Abate, U. Steiner, M. Grätzel, M. E. Calvo, A. Hagfeldt, H. Míguez, *J. Mater. Chem. A* **2016**, *60*, 269.
[55] Z. Yang, A. Rajagopal, C. C. Chueh, S. B. Jo, B. Liu, T. Zhao, A. K. Y. Jen, *Adv. Mater.* **2016**, *28*, 8990.
[56] G. E. Eperon, T. Leijtens, K. A. Bush, R. Prasanna, T. Green, J. T.-W. Wang, D. P. McMeekin, G. Volonakis, R. L. Milot, R. May, A. Palmstrom, D. J. Slotcavage, R. A. Belisle, J. B. Patel, E. S. Parrott, R. J. Sutton, W. Ma, F. Moghadam, B. Conings, A. Babayigit, H.-G. Boyen, S. Bent, F. Giustino, L. M. Herz, M. B. Johnston, M. D. McGehee, H. J. Snaith, *Science* **2016**, *354*, 861.
[57] D. Zhao, Y. Yu, C. Wang, W. Liao, N. Shrestha, C. R. Grice, A. J. Cimaroli, L. Guan, R. J. Ellingson, K. Zhu, X. Zhao, R.-G. Xiong, Y. Yan, *Nat. Energy* **2017**, *2*, 17018.
[58] S. Essig, J. Benick, M. Schachtner, A. Wekkeli, M. Hermle, F. Dimroth, *IEEE J. Photovoltaics* **2015**, *5*, 977.
[59] D. C. Bobela, L. Gedvilas, M. Woodhouse, K. A. W. Horowitz, P. A. Basore, *Prog. Photovoltaics* **2017**, *25*, 41.
[60] D. B. Mitzi, C. A. Feild, W. T. A. Harrison, A. M. Guloy, *Nature* **1994**, *369*, 467.
[61] A. Kojima, K. Teshima, Y. Shirai, T. Miyasaka, *J. Am. Chem. Soc.* **2009**, *131*, 6050.
[62] M. M. Lee, J. Teuscher, T. Miyasaka, T. N. Murakami, H. J. Snaith, *Science* **2012**, *338*, 643.
[63] M. Liu, M. B. Johnston, H. J. Snaith, *Nature* **2013**, *501*, 395.
[64] H. J. Snaith, *J. Phys. Chem. Lett.* **2013**, *4*, 3623.
[65] P. Löper, B. Niesen, S.-J. Moon, S. Martin de Nicolas, J. Holovsky, Z. Remes, M. Ledinsky, F.-J. Haug, J.-H. Yum, S. De Wolf, C. Ballif, *IEEE J. Photovoltaics* **2014**, *4*, 1545.
[66] B. W. Schneider, N. N. Lal, S. Baker-Finch, T. P. White, *Opt. Express* **2014**, *22*, A1422.
[67] S. Albrecht, M. Saliba, J.-P. Correa-Baena, K. Jäger, L. Korte, A. Hagfeldt, M. Grätzel, B. Rech, *J. Opt.* **2016**, *18*, 64012.
[68] P. Löper, S.-J. Moon, S. Martín de Nicolas, B. Niesen, M. Ledinsky, S. Nicolay, J. Bailat, J.-H. Yum, S. De Wolf, C. Ballif, *Phys. Chem. Chem. Phys.* **2015**, *17*, 1619.
[69] C. D. Bailie, M. G. Christoforo, J. P. Mailoa, A. R. Bowring, E. L. Unger, W. H. Nguyen, J. Burschka, N. Pellet, J. Z. Lee, M. Grätzel, R. Noufi, T. Buonassisi, A. Salleo, M. D. McGehee, *Energy Environ. Sci.* **2014**, *8*, 956.
[70] J. Werner, G. Dubuis, A. Walter, P. Löper, S.-J. Moon, S. Nicolay, M. Morales-Masis, S. De Wolf, B. Niesen, C. Ballif, *Sol. Energy Mater. Sol. Cells* **2015**, *141*, 407.
[71] J. P. Mailoa, C. D. Bailie, E. C. Johlin, E. T. Hoke, A. J. Akey, W. H. Nguyen, M. D. McGehee, T. Buonassisi, *Appl. Phys. Lett.* **2015**, *106*, 121105.
[72] J. Werner, L. Barraud, A. Walter, M. Bräuninger, F. Sahli, D. Sacchetto, N. Tétreault, B. Paviet-Salomon, S.-J. Moon, C. Allebé, M. Despeisse, S. Nicolay, S. De Wolf, B. Niesen, C. Ballif, *ACS Energy Lett.* **2016**, *1*, 474.
[73] K. A. Bush, A. F. Palmstrom, Z. (Jason) Yu, M. Boccard, R. Cheacharoen, J. P. Mailoa, D. P. McMeekin, R. L. Z. Hoye, C. D. Bailie, T. Leijtens, I. M. Peters, M. C. Minichetti, N. Rolston, R. Prasanna, S. E. Sofia, D. Harwood, W. Ma, F. Moghadam, H. J. Snaith, T. Buonassisi, Z. C. Holman, S. F. Bent, M. D. McGehee, *Nat. Energy* **2017**, *2*, 17009.
[74] D. P. McMeekin, G. Sadoughi, W. Rehman, G. E. Eperon, M. Saliba, M. T. Horantner, A. Haghighirad, N. Sakai, L. Korte, B. Rech, M. B. Johnston, L. M. Herz, H. J. Snaith, *Science* **2016**, *351*, 151.
[75] T. Duong, N. Lal, D. Grant, D. Jacobs, P. Zheng, S. Rahman, H. Shen, M. Stocks, A. Blakers, K. Weber, T. P. White, K. R. Catchpole, *IEEE J. Photovoltaics* **2016**, *6*, 679.
[76] B. Chen, Y. Bai, Z. Yu, T. Li, X. Zheng, Q. Dong, L. Shen, M. Boccard, A. Gruverman, Z. Holman, J. Huang, *Adv. Energy Mater.* **2016**, *6*, 1601128.
[77] J. Peng, T. Duong, X. Zhou, H. Shen, Y. Wu, H. K. Mulmudi, Y. Wan, D. Zhong, J. Li, T. Tsuzuki, K. J. Weber, K. R. Catchpole, T. P. White, *Adv. Energy Mater.* **2017**, *7*, 1601768.
[78] T. Duong, Y. Wu, H. Shen, J. Peng, X. Fu, D. Jacobs, E. Wang, T. C. Kho, K. C. Fong, M. Stocks, E. Franklin, A. Blakers, N. Zin, K. McIntosh, W. Li, Y. Cheng, T. P. White, K. Weber, K. Catchpole, *Adv. Energy Mater.* **2017**, *7*, 1700228.
[79] M. Jaysankar, W. Qiu, M. van Eerden, T. Aernouts, R. Gehlhaar, M. Debucquoy, U. W. Paetzold, J. Poortmans, *Adv. Energy Mater.* **2017**, *7*, 1602807.
[80] S. Albrecht, M. Saliba, J. P. Correa Baena, F. Lang, L. Kegelmann, M. Mews, L. Steier, A. Abate, J. Rappich, L. Korte, R. Schlatmann, N. Mohammad, K. A. Hagfeldt, M. Grätzel, B. Rech, *Energy Environ. Sci.* **2016**, *9*, 81.
[81] J. Werner, C.-H. Weng, A. Walter, L. Fesquet, J. P. Seif, S. De Wolf, B. Niesen, C. Ballif, *J. Phys. Chem. Lett.* **2016**, *7*, 161.
[82] J. Werner, A. Walter, E. Rucavado, S.-J. Moon, D. Sacchetto, M. Rienaecker, R. Peibst, R. Brendel, X. Niquille, S. De Wolf, P. Löper, M. Morales-Masis, S. Nicolay, B. Niesen, C. Ballif, *Appl. Phys. Lett.* **2016**, *109*, 233902.
[83] F. Sahli, B. Kamino, J. Werner, M. Bräuninger, B. Paviet-Salomon, L. Barraud, R. Monnard, J. P. Seif, A. Tomasi, Q. Jeangros, A. Hessler-Wyser, S. De Wolf, M. Despeisse, S. Nicolay, B. Niesen, C. Ballif, *Adv. Energy Mater.*, **2017**, unpublished.
[84] M. Saliba, T. Matsui, J.-Y. Seo, K. Domanski, J.-P. Correa-Baena, N. Mohammad, K. S. M. Zakeeruddin, W. Tress, A. Abate, A. Hagfeldt, M. Gratzel, *Energy Environ. Sci.* **2016**, *9*, 1989.
[85] K. A. Bush, C. D. Bailie, Y. Chen, T. Leijtens, A. R. Bowring, F. Moghadam, M. D. McGehee, *Adv. Mater.* **2016**, *28*, 3937.
[86] J. Werner, F. Sahli, B. Kamino, D. Sacchetto, M. Bräuninger, A. Walter, S. Moon, L. Barraud, B. Paviet-Salomon, J. Geissbuehler, C. Allebé, R. Monnard, S. De Wolf, M. Despeisse, S. Nicolay, B. Niesen, C. Ballif, in *IEEE-PVSC Conf. Proc.*, IEEE, Washington, DC **2017**.
[87] R. Fan, Y. Huang, L. Wang, L. Li, G. Zheng, H. Zhou, *Adv. Energy Mater.* **2016**, *6*, 1.

[88] J. H. Kim, C.-C. Chueh, S. T. Williams, A. K.-Y. Jen, *Nanoscale* **2015**, *7*, 17343.
[89] C. Tao, S. Neutzner, L. Colella, S. Marras, A. R. Srimath Kandada, M. Gandini, M. De Bastiani, G. Pace, L. Manna, M. Caironi, C. Bertarelli, A. Petrozza, *Energy Environ. Sci.* **2015**, *8*, 8.
[90] E. H. Anaraki, A. Kermanpur, L. Steier, K. Domanski, T. Matsui, W. Tress, M. Saliba, A. Abate, M. Grä, A. Hagfeldt, J.-P. Correa-Baena, *Energy Environ. Sci.* **2016**, *9*, 3128.
[91] L. Calio, S. Kazim, M. Graetzel, S. Ahmad, *Angew. Chem., Int. Ed.* **2016**, *55*, 14522.
[92] R. Rajeswari, M. Mrinalini, S. Prasanthkumar, L. Giribabu, *Chem. Rec.* **2017**, *17*, 1.
[93] M. Morales-Masis, S. De Wolf, R. Woods-Robinson, J. W. Ager, C. Ballif, *Adv. Electron. Mater.* **2017**, *3*, 1600529.
[94] F. Lang, M. A. Gluba, S. Albrecht, O. Shargaieva, J. Rappich, L. Korte, B. Rech, N. H. Nickel, *Phys. Status Solidi* **2016**, *213*, 1989.
[95] F. Lang, M. A. Gluba, S. Albrecht, J. Rappich, L. Korte, B. Rech, N. H. Nickel, *J. Phys. Chem. Lett.* **2015**, *6*, 2745.
[96] F. Guo, H. Azimi, Y. Hou, T. Przybilla, M. Hu, C. Bronnbauer, S. Langner, E. Spiecker, K. Forberich, C. J. Brabec, *Nanoscale* **2014**, *7*, 1642.
[97] J. Werner, J. Geissbuehler, A. Dabirian, S. Nicolay, M. Morales Masis, S. De Wolf, B. Niesen, C. Ballif, J. Geissbühler, A. Dabirian, S. Nicolay, M. Morales-Masis, S. D. Wolf, B. Niesen, C. Ballif, *ACS Appl. Mater. Interfaces* **2016**, *8*, 27.
[98] J. Ahn, H. Hwang, S. Jeong, J. Moon, *Adv. Energy Mater.* **2017**, *7*, 1602751.
[99] Y. Kato, L. K. Ono, M. V. Lee, S. Wang, S. R. Raga, Y. Qi, *Adv. Mater. Interfaces* **2015**, *2*, 2.
[100] P. You, Z. Liu, Q. Tai, S. Liu, F. Yan, *Adv. Mater.* **2015**, *27*, 3632.
[101] H. Kanda, A. Uzum, H. Nishino, T. Umeyama, H. Imahori, Y. Ishikawa, Y. Uraoka, S. Ito, *ACS Appl. Mater. Interfaces* **2016**, *8*, 33553.
[102] J. Werner, S.-J. Moon, P. Löper, M. Filipic, C.-H. Weng, L. Löfgren, J. Bailat, M. Topic, M. Morales-Masis, R. Peibst, R. Brendel, S. Nicolay, S. De Wolf, B. Niesen, C. Ballif, presented at *31st European PV Solar Conf. and Exhibition*, Hamburg, Germany, September **2015**.
[103] M. Filipic, P. Löper, B. Niesen, S. De Wolf, J. Krc, C. Ballif, M. Topic, *Opt. Express* **2015**, *23*, 263.
[104] C. Momblona, L. Gil-Escrig, E. Bandiello, E. M. Hutter, M. Sessolo, K. Lederer, J. Blochwitz-Nimoth, H. J. Bolink, *Energy Environ. Sci.* **2016**, *9*, 3456.
[105] R. A. Belisle, P. Jain, R. Prasanna, T. Leijtens, M. D. McGehee, *ACS Energy Lett.* **2016**, *1*, 556.
[106] J. W. Jung, C.-C. Chueh, A. K.-Y. Jen, *Adv. Energy Mater.* **2015**, *5*, 1500486.
[107] J. Liu, S. K. Pathak, N. Sakai, R. Sheng, S. Bai, Z. Wang, H. J. Snaith, *Adv. Mater. Interfaces* **2016**, *3*, 1.
[108] W. Ke, D. Zhao, C. R. Grice, A. J. Cimaroli, G. Fang, Y. Yan, *J. Mater. Chem. A* **2015**, *3*, 23888.
[109] R. Santbergen, R. Mishima, T. Meguro, M. Hino, H. Uzu, J. Blanker, K. Yamamoto, M. Zeman, *Opt. Express* **2016**, *24*, A1288.
[110] K. Jäger, L. Korte, B. Rech, S. Albrecht, *Opt. Express* **2017**, *25*, A473.
[111] G. E. Eperon, S. D. Stranks, C. Menelaou, M. B. Johnston, L. M. Herz, H. J. Snaith, *Energy Environ. Sci.* **2014**, *7*, 982.
[112] B. Brunetti, C. Cavallo, A. Ciccioli, G. Gigli, A. Latini, *Sci. Rep.* **2016**, *6*, 31896.
[113] E. T. Hoke, D. J. Slotcavage, E. R. Dohner, A. R. Bowring, H. I. Karunadasa, M. D. McGehee, *Chem. Sci.* **2015**, *6*, 613.
[114] D. J. Slotcavage, H. I. Karunadasa, M. D. McGehee, *ACS Energy Lett.* **2016**, *1*, 1199.
[115] A. J. Barker, A. Sadhanala, F. Deschler, M. Gandini, S. P. Senanayak, P. M. Pearce, E. Mosconi, A. J. Pearson, Y. Wu, A. R. Srimath Kandada, T. Leijtens, F. De Angelis, S. E. Dutton, A. Petrozza, R. H. Friend, *ACS Energy Lett.* **2017**, *2*, 1416.
[116] R. E. Beal, D. J. Slotcavage, T. Leijtens, A. R. Bowring, R. A. Belisle, W. H. Nguyen, G. Burkhard, E. T. Hoke, M. D. McGehee, *J. Phys. Chem. Lett.* **2016**, *7*, 746.
[117] W. Ahmad, J. Khan, G. Niu, J. Tang, *Sol. RRL* **2017**, *1*, 1700048.
[118] L. A. Frolova, D. V. Anokhin, A. A. Piryazev, S. Y. Luchkin, N. N. Dremova, K. J. Stevenson, P. A. Troshin, *J. Phys. Chem. Lett.* **2017**, *8*, 67.
[119] Y. Lin, B. Chen, F. Zhao, X. Zheng, Y. Deng, Y. Shao, Y. Fang, Y. Bai, C. Wang, J. Huang, *Adv. Mater.* **2017**, *29*, 1700607.
[120] M. Bonnet-Eymard, M. Boccard, G. Bugnon, F. Sculati-Meillaud, M. Despeisse, C. Ballif, *Sol. Energy Mater. Sol. Cells* **2013**, *117*, 120.
[121] Q. Lin, A. Armin, R. C. R. Nagiri, P. L. Burn, P. Meredith, *Nat. Photonics* **2015**, *9*, 106.
[122] A. Mahboubi Soufiani, Y. Zhuo, T. Young, A. Miyata, A. Surrente, A. R. Pascoe, K. Galkowski, M. Abdi-Jalebi, R. Brenes, J. Urban, N. Zhang, V. Bulovic, O. Portugall, Y.-B. Cheng, R. J. Nicholas, A. W. Y. Ho-Baillie, M. Green, P. Plochocka, S. D. Stranks, *Energy Environ. Sci.* **2017**, *10*, 1358.
[123] Z. Song, J. Werner, N. Shrestha, F. Sahli, S. De Wolf, B. Niesen, S. C. Watthage, A. B. Phillips, C. Ballif, R. J. Ellingson, M. J. Heben, *J. Phys. Chem. Lett.* **2016**, *7*, 5114.
[124] L. E. Mundt, F. D. Heinz, S. Albrecht, M. Mundus, M. Saliba, J. P. Correa-Baena, E. H. Anaraki, L. Korte, M. Grätzel, A. Hagfeldt, B. Rech, M. C. Schubert, S. W. Glunz, *IEEE J. Photovoltaics* **2017**, *7*, 1081.
[125] G. El-Hajje, C. Momblona, L. Gil-Escrig, J. Ávila, T. Guillemot, J.-F. Guillemoles, M. Sessolo, H. J. Bolink, L. Lombez, *Energy Environ. Sci.* **2016**, *131*, 6050.
[126] T. Söderström, F. J. Haug, X. Niquille, V. Terrazzoni, C. Ballif, *Appl. Phys. Lett.* **2009**, *94*, 1.
[127] F.-J. Haug, C. Ballif, *Energy Environ. Sci.* **2010**, *8*, 824.
[128] S. Essig, M. A. Steiner, C. Allebé, J. F. Geisz, B. Paviet-salomon, S. Ward, A. Descoeudres, V. Lasalvia, L. Barraud, N. Badel, A. Faes, J. Levrat, M. Despeisse, C. Ballif, P. Stradins, D. L. Young, *IEEE J. Photovoltaics* **2016**, *6*, 1012.
[129] D.-L. Wang, H.-J. Cui, G.-J. Hou, Z.-G. Zhu, Q.-B. Yan, G. Su, *Sci. Rep.* **2016**, *6*, 18922.
[130] N.-F. Wang, T.-W. Kuo, Y.-Z. Tsai, S.-X. Lin, P.-K. Hung, C.-L. Lin, M.-P. Houng, *Opt. Express* **2012**, *20*, 7445.
[131] J. Zhang, J. Li, L. Zheng, Y. Lu, E. Moulin, F. Haug, C. Ballif, H. Xu, N. Dai, W. Song, *Sol. Energy Mater. Sol. Cells* **2015**, *143*, 546.
[132] J. Escarré, K. Söderström, M. Despeisse, S. Nicolay, C. Battaglia, G. Bugnon, L. Ding, F. Meillaud, F. J. Haug, C. Ballif, *Sol. Energy Mater. Sol. Cells* **2012**, *98*, 185.
[133] C. Ulbrich, A. Gerber, K. Hermans, A. Lambertz, U. Rau, *Prog. Photovoltaics* **2013**, *21*, 1672.
[134] M. Jošt, S. Albrecht, L. Kegelmann, C. M. Wolff, F. Lang, B. Lipovsek, J. Krč, L. Korte, D. Neher, B. Rech, M. Topič, *ACS Photonics* **2017**, *4*, 1232.
[135] Y. Peng, H. Huang, H. Xie, *Sol. Energy Mater. Sol. Cells* **2017**, *171*, 98.
[136] S. Manzoor, Z. J. Yu, A. Ali, W. Ali, K. A. Bush, A. F. Palmstrom, S. F. Bent, M. D. McGehee, Z. C. Holman, *Sol. Energy Mater. Sol. Cells* **2017**, https://doi.org/10.1016/j.solmat.2017.06.020.
[137] D. Shi, Y. Zeng, W. Shen, *Sci. Rep.* **2015**, *5*, 16504.
[138] J. Chen, X. Cai, D. Yang, D. Song, J. Wang, J. Jiang, A. Ma, S. Lv, M. Z. Hu, C. Ni, *J. Power Sources* **2017**, *355*, 98.
[139] T. Leijtens, K. Bush, R. Cheacharoen, R. Beal, A. Bowring, M. D. McGehee, *J. Mater. Chem. A* **2017**, *5*, 11483.
[140] C. Quarti, E. Mosconi, J. M. Ball, V. D'Innocenzo, C. Tao, S. Pathak, H. J. Snaith, A. Petrozza, F. De Angelis, *Energy Environ. Sci.* **2016**, *9*, 155.

[141] B. Conings, J. Drijkoningen, N. Gauquelin, A. Babayigit, J. D'Haen, L. D'Olieslaeger, A. Ethirajan, J. Verbeeck, J. Manca, E. Mosconi, F. De Angelis, H.-G. Boyen, *Adv. Energy Mater.* **2015**, *5*, 1500477.
[142] C. C. Stoumpos, C. D. Malliakas, M. G. Kanatzidis, *Inorg. Chem.* **2013**, *52*, 9019.
[143] O. A. Syzgantseva, M. Saliba, M. Grätzel, U. Rothlisberger, *J. Phys. Chem. Lett.* **2017**, *8*, 1191.
[144] J. Huang, P. Xu, J. Liu, X. You, *Small* **2017**, *13*, 1603225.
[145] T. Duong, H. K. Mulmudi, H. Shen, Y. L. Wu, C. Barugkin, Y. O. Mayon, H. T. Nguyen, D. Macdonald, J. Peng, M. Lockrey, W. Li, Y. B. Cheng, T. P. White, K. Weber, K. Catchpole, *Nano Energy* **2016**, *30*, 330.
[146] T. J. Jacobsson, W. Tress, J.-P. Correa-Baena, T. Edvinsson, A. Hagfeldt, *J. Phys. Chem. C* **2016**, *120*, 11382.
[147] Z. Song, A. Abate, S. C. Watthage, G. K. Liyanage, A. B. Phillips, U. Steiner, M. Graetzel, M. J. Heben, *Adv. Energy Mater.* **2016**, *6*, 1600846.
[148] Z. Wang, D. P. McMeekin, N. Sakai, S. van Reenen, K. Wojciechowski, J. B. Patel, M. B. Johnston, H. J. Snaith, *Adv. Mater.* **2017**, *29*, 1604186.
[149] Z. Li, M. Yang, J. S. Park, S. H. Wei, J. J. Berry, K. Zhu, *Chem. Mater.* **2016**, *28*, 284.
[150] W. Li, H. Dong, L. Wang, N. Li, X. Guo, J. Li, Y. Qiu, *J. Mater. Chem. A* **2014**, *2*, 13587.
[151] T. Malinauskas, D. Tomkute-Luksiene, R. Sens, M. Daskeviciene, R. Send, H. Wonneberger, V. Jankauskas, I. Bruder, V. Getautis, *ACS Appl. Mater. Interfaces* **2015**, *7*, 11107.
[152] J. Yang, B. D. Siempelkamp, E. Mosconi, F. De Angelis, T. L. Kelly, *Chem. Mater.* **2015**, *27*, 4229.
[153] L. Zhao, R. A. Kerner, Z. Xiao, Y. L. Lin, K. M. Lee, J. Schwartz, B. P. Rand, *ACS Energy Lett.* **2016**, *1*, 595.
[154] K. Domanski, J. P. Correa-Baena, N. Mine, M. K. Nazeeruddin, A. Abate, M. Saliba, W. Tress, A. Hagfeldt, M. Graetzel, *ACS Nano* **2016**, *10*, 6306.
[155] E. M. Sanehira, B. J. Tremolet de Villers, P. Schulz, M. O. Reese, S. Ferrere, K. Zhu, L. Y. Lin, J. J. Berry, J. M. Luther, *ACS Energy Lett.* **2016**, *1*, 38.
[156] P. Schulz, J. O. Tiepelt, J. A. Christians, I. Levine, E. Edri, E. M. Sanehira, G. Hodes, D. Cahen, A. Kahn, *ACS Appl. Mater. Interfaces* **2016**, *8*, 31491.
[157] K. O. Brinkmann, J. Zhao, N. Pourdavoud, T. Becker, T. Hu, S. Olthof, K. Meerholz, L. Hoffmann, T. Gahlmann, R. Heiderhoff, M. F. Oszajca, N. A. Luechinger, D. Rogalla, Y. Chen, B. Cheng, T. Riedl, *Nat. Commun.* **2017**, *8*, 13938.
[158] J. Zhao, K. O. Brinkmann, T. Hu, N. Pourdavoud, T. Becker, T. Gahlmann, R. Heiderhoff, A. Polywka, P. Görrn, Y. Chen, B. Cheng, T. Riedl, *Adv. Energy Mater.* **2017**, *7*, 1602599.
[159] L. Shi, T. L. Young, J. Kim, Y. Sheng, L. Wang, Y. Chen, Z. Feng, M. Keevers, X. Hao, P. Verlinden, M. A. Green, A. W. Y. Ho-Baillie, *ACS Appl. Mater. Interfaces* **2017**, *9*, 25073.
[160] IEC, *IEC International Standard for design qualification and type approval of PV modules, IEC 61215*, International Electrotechnical Commission, **2016**.
[161] D. Kirk, *"Perockite/Silicon Tandem Cells" in Hercules Projectworkshop*, Helmholtz-Zentrum Berlin, Germany **2016** (https://www.helmholtz-berlin.de/projects/hercules/2nd-hercules-workshop/programme_en.html).
[162] W. Chen, Y. Wu, Y. Yue, J. Liu, W. Zhang, X. Yang, H. Chen, E. Bi, I. Ashraful, M. Grätzel, L. Han, *Science* **2015**, *350*, 944.
[163] X. Li, D. Bi, C. Yi, J.-D. Decoppet, J. Luo, S. M. Zakeeruddin, A. Hagfeldt, M. Gratzel, *Science* **2016**, *8060*, 1.
[164] Y. Hu, S. Si, A. Mei, Y. Rong, H. Liu, X. Li, H. Han, *Sol. RRL* **2017**, *1*, 1600019.
[165] S.-J. Moon, J.-H. Yum, L. Lofgren, A. Walter, L. Sansonnens, M. Benkhaira, S. Nicolay, J. Bailat, C. Ballif, *IEEE J. Photovoltaics* **2015**, *5*, 1087.
[166] G. D. Spyropoulos, C. O. R. Quiroz, M. Salvador, Y. Hou, N. Gasparini, P. Schweizer, J. Adams, P. Kubis, N. Li, E. Spiecker, T. Ameri, H.-J. Egelhaaf, C. J. Brabec, *Energy Environ. Sci.* **2016**, *9*, 13.
[167] L. Rakocevic, R. Gehlhaar, T. Merckx, W. Qui, U. W. Paetzold, H. Fledderus, J. Poortmans, *IEEE J. Photovoltaics* **2016**, *7*, 404.
[168] W. Qiu, A. Ray, M. Jaysankar, T. Merckx, J. P. Bastos, D. Cheyns, R. Gehlhaar, J. Poortmans, P. Heremans, *Adv. Funct. Mater.* **2017**, *27*, 1700920.
[169] G. Grancini, I. Zimmermann, E. Mosconi, D. Martineau, S. Narbey, *Nat. Commun.* **2017**, *8*, 15684.
[170] Z. Song, C. Mcelvany, A. B. Phillips, I. Celik, P. Krantz, S. C. Watthage, G. K. Liyanage, D. Apu, M. Heben, *Energy Environ. Sci.* **2017**, *10*, 1297.
[171] L. Gil-Escrig, C. Momblona, D. Forgács, S. Pla, F. Fernández-Lázaro, M. Sessolo, Á. Sastre-Santos, H. J. Bolink, *Org. Electron.* **2016**, *37*, 396.
[172] A. Ng, Z. Ren, Q. Shen, S.-H. Cheung, H. C. Gokkaya, S. K. So, A. B. Djurisic, Y. Wan, X. Wu, C. Surya, *ACS Appl. Mater. Interfaces* **2016**, *8*, 32805.
[173] A. Ioakeimidis, C. Christodoulou, M. Lux-Steiner, K. Fostiropoulos, *J. Solid State Chem.* **2016**, *244*, 20.
[174] J. Geissbühler, S. De Wolf, A. Faes, N. Badel, Q. Jeangros, A. Tomasi, L. Barraud, A. Descoeudres, M. Despeisse, C. Ballif, *IEEE J. Photovoltaics* **2014**, *4*, 1055.
[175] A. Babayigit, A. Ethirajan, M. Muller, B. Conings, *Nat. Mater.* **2016**, *15*, 247.
[176] F. Giustino, H. J. Snaith, *ACS Energy Lett.* **2016**, *1*, 1233.
[177] S. Yang, W. Fu, Z. Zhang, H. Chen, C.-Z. Li, *J. Mater. Chem. A* **2017**, *5*, 11462.
[178] I. M. Peters, S. Sofia, J. Mailoa, T. Buonassisi, *RSC Adv.* **2016**, *6*, 66911.
[179] N. L. Chang, A. W. Yi Ho-Baillie, P. A. Basore, T. L. Young, R. Evans, R. J. Egan, *Prog. Photovoltaics* **2017**, *25*, 390.
[180] N. M. Haegel, R. Margolis, T. Buonassisi, D. Feldman, A. Froitzheim, R. Garabedian, M. Green, S. Glunz, H.-M. Henning, B. Holder, I. Kaizuka, B. Kroposki, K. Matsubara, S. Niki, K. Sakurai, R. A. Schindler, M. Woodhouse, S. Kurtz, *Science* **2017**, *356*, 141.

